Mar Geophys Res (2016) 37:71–94
DOI 10.1007/s11001-016-9266-3

ORIGINAL RESEARCH PAPER

Cenozoic magmatism in the northern continental margin of the South China Sea: evidence from seismic profiles

Qiao Zhang[1,2,3] · Shiguo Wu[1] · Dongdong Dong[1]

Received: 21 July 2015 / Accepted: 8 March 2016 / Published online: 18 March 2016

Abstract Igneous rocks in the northern margin of the South China Sea (SCS) have been identified via high resolution multi-channel seismic data in addition to other geophysical and drilling well data. This study identified intrusive and extrusive structures including seamounts and buried volcanoes, and their seismic characteristics. Intrusive features consist of piercement and implicit-piercement type structures, indicating different energy input associated with diapir formation. Extrusive structures are divided into flat-topped and conical-topped seamounts. Three main criteria (the overlying strata, the contact relationship and sills) were used to distinguish between intrusive rocks and buried volcanos. Three criteria are also used to estimate the timing of igneous rock formation: the contact relationship, the overlying sedimentary thickness and seismic reflection characteristics. These criteria are applied to recognize and distinguish between three periods of Cenozoic magmatism in the northern margin of the SCS: before seafloor spreading (Paleocene and Eocene), during seafloor spreading (Early Oligocene–Mid Miocene) and after cessation of seafloor spreading (Mid Miocene–Recent). Among them, greater attention is given to the extensive magmatism since 5.5 Ma, which is present throughout nearly all of the study area, making it a significant event in the SCS. Almost all of the Cenozoic igneous rocks were located below the 1500 m bathymetric contour. In contrast with the wide distribution of igneous rocks in the volcanic rifted margin, igneous rocks in the syn-rift stage of the northern margin of the SCS are extremely sporadic, and they could only be found in the southern Pearl River Mouth basin and NW sub-sea basin. The ocean–continent transition of the northern SCS exhibits high-angle listric faults, concentrated on the seaward side of the magmatic zone, and a sharply decreased crust, with little influence from a mantle plume. These observations provide further evidence to suggest that the northern margin of the SCS is a magma-poor rifted margin.

Keywords Igneous rock · Seismic imaging · Passive continental margin · South China Sea

✉ Dongdong Dong
dongdongdong@qdio.ac.cn

[1] Key Laboratory of Marine Geology and Environment, Institute of Oceanology, CAS, Qingdao 266071, China

[2] University of Chinese Academy of Sciences, Beijing 100049, China

[3] Key Laboratory of Submarine Geosciences, Second Institute of Oceanography, State Oceanic Administration, Hangzhou 310012, China

Introduction

Magmatism plays an important role in plate reconstruction and regional tectonic evolution. Recently, considerable attention has been focused on magmatism in passive continental margins. Passive continental margins can be divided into magma-rich volcanic continental margins, such as the margins located along the South Atlantic Ocean and the Norwegian margin (White and McKenzie 1989; Planke et al. 2000; Franke et al. 2014), and magma-poor (non-volcanic) rifted margins, such as the Alpine Tethys and Iberia-Newfoundland rifted margins (Dean et al. 2000; Péron-Pinvidic et al. 2007; Mohn et al. 2012; Franke et al. 2014). Continued research on magmatism and magmatic processes is important because it improves our understanding of continental rifting, seafloor spreading and the

formation of deep water basins along passive margins (Yan et al. 2006; Shi and Yan 2011).

The early rifting history of the South China Sea (SCS) spans from the Late Cretaceous to the Early Paleogene. Late Mesozoic to Recent igneous rocks have been found in the northern margin of the SCS (Zhou and Li 2000; Zhou et al. 2006; Yan et al. 2006; Fig. 1). A lithological study has been carried out on drilled and dredged rock samples (Kudrass et al. 1986; Ru and Pigott 1986; Rao and Li 1991; Li and Rao 1994; Zhou et al. 2005; Yan et al. 2006), but shortage of samples limited the study range in space. Geophysical methods are crucial in order to provide a regional perspective. As indicated by gravitational and magnetic anomalies, igneous rocks are considered to be widely distributed in the SCS (Briais et al. 1993; Yao et al. 1994; Wan et al. 2006; Meng et al. 2009; Li et al. 2010). Furthermore, igneous rocks were found in more than 20 wells on the northern margin of the SCS (Ru and Pigott 1986; Rao and Li 1991; Li and Rao 1994). However, the pre-existing seismic analyses are insufficient and unsystematic, leading to the ambiguity about the detailed features, distribution and formation time of the igneous rocks in the SCS area.

This study focuses on identifying the seismic characteristics and distribution of Cenozoic igneous rocks in the

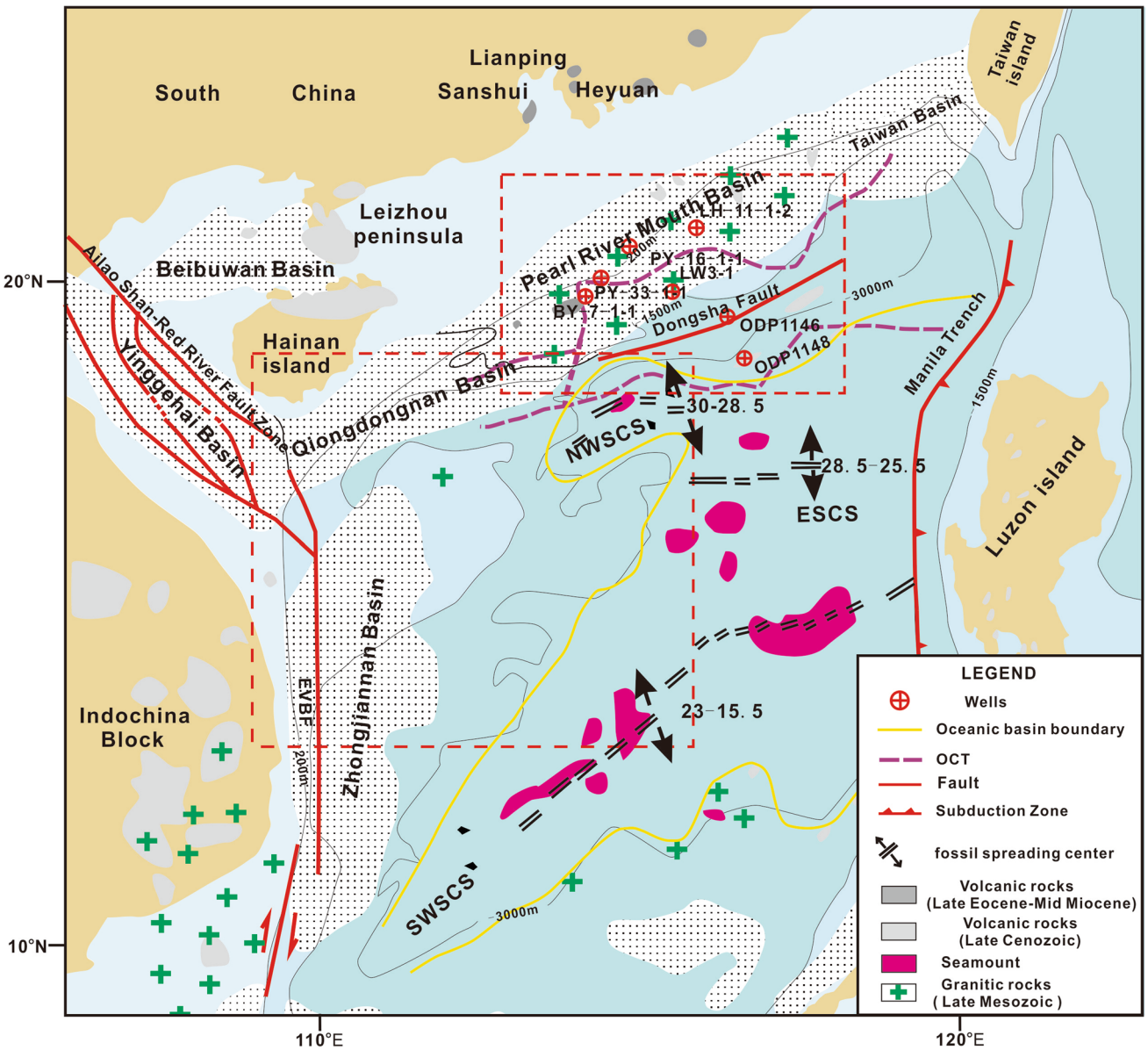

Fig. 1 Tectonic framework of the South China Sea illustrating the distribution of igneous rocks and major Cenozoic rifted basins (modified after Ru and Pigott 1986; Tapponnier et al. 1986; Lüdmann and Wong 1999; Yan et al. 2006; Sun et al. 2009; Yan et al. 2014). *SWSCS* Southwest South China Sea, *NWSCS* Northwest South China Sea, *ESCS:*East South China Sea

northern margin of the SCS (Fig. 2). A large number of seismic profiles and drilling data, obtained from 2002 to 2011, are re-analyzed in order to deepen our understanding of magmatism in the northern SCS.

Geological background

The SCS is located at the intersection of the Eurasian plate, the Pacific plate and the Indo-Australian plate, making it one of the largest marginal sea basins of the western Pacific. Boundary types vary in each direction (Fig. 1): a broad passive margin to the north, a collision zone along the Palawan trough to the south, the narrow Indo-china shelf with large strike-slip faults to the west and the subduction zone along the Manila trench to the east (Tapponnier et al. 1982, 1986; Yan and Shi 2007; Clift et al. 2008). Several models have been proposed to interpret the opening of the SCS (Taylor and Hayes 1983; Tapponnier et al. 1982, 1986; Chung et al. 1997; Dong et al. 2014). Continental rifting likely began in the Late Cretaceous or the early Paleocene (Holloway 1982; Taylor and Hayes 1983; Hinz and Schlüter 1985; Lee and Watkins 1998). This has been confirmed by the recent deep tow magnetic survey and IODP expedition 349 in the SCS (Li et al. 2014).

The northern margin of the SCS has been influenced by Pacific plate subduction in the Mesozoic and rifting in the Cenozoic (Taylor and Hayes 1983; Charvet et al. 1994; Shi and Li 2012; Franke et al. 2014). Since the Late Cenozoic, several geological events, such as the Indochina block extrusion (Tapponnier et al. 1982, 1986), seafloor spreading (Briais et al. 1993; Barckhausen and Roeser 2004), the SCS subduction beneath the Manila trench (Holloway 1982; Lüdmann et al. 2001), and the Taiwan orogenic event (Jahn et al. 1990; Zou 1993), have resulted in intensive magmatism and tectonic activity (Pigott and Ru

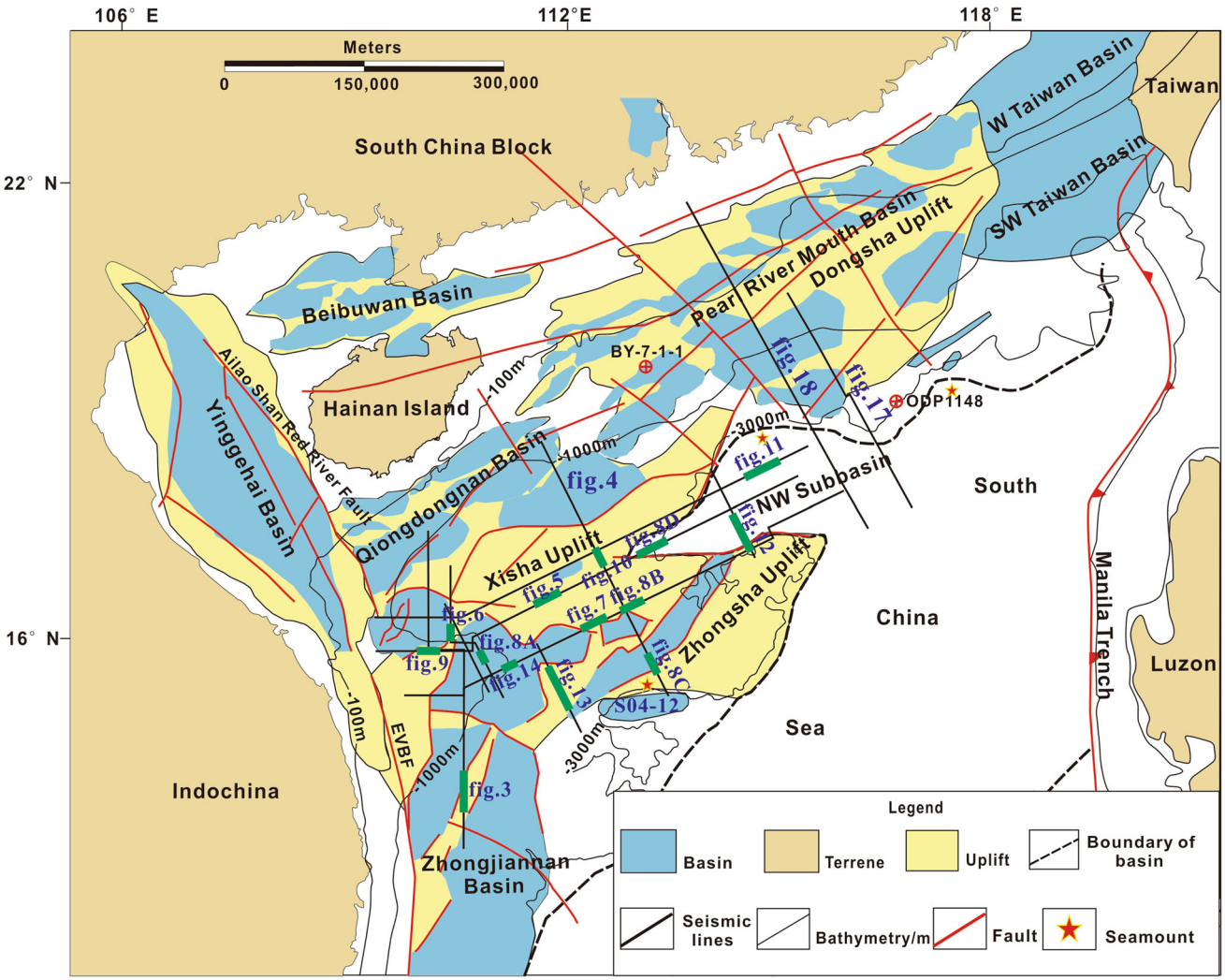

Fig. 2 Tectonic units of the northern margin of the SCS. Black seismic profiles are used in this study. *Green bold lines* are portions of seismic data shown in this paper. *Red circles* show the locations of ODP/IODP site 1148, and industrial borehole BY 7-1-1 (Zou et al. 1995; Qin 2007)

1994). Igneous rocks, formed intermittently from the Late Mesozoic to recent, have been found extensively along the northern SCS margin. The drilled rock samples provide evidence for different lithological compositions with age (Fig. 1). Felsic igneous rocks comprise the majority of those formed during the Mesozoic, however, the intermediate-basalt component subsequently increased through the Paleocene and Eocene. Since the Miocene, mafic basalt is the primary type of igneous rock observed along the northern margin of the SCS (Yan et al. 2006).

Data and methods

An extensive multi-channel seismic reflection dataset extending from the continental shelf to the oceanic basin of the study areas was acquired from 2002 to 2011 (Fig. 2). Seismic processing of this dataset included amplitude compensation, multiple attenuation, velocity analysis, correction, and finite-difference migration. The Common Middle Point (CMP) spacing is 12.5 m and the frequency bandwidth ca. 30–45 Hz, with vertical resolution ca. 25 m (Sun et al. 2011).

Seismic data provides a powerful alternative method for studying magmatism, because buried volcanic structures can be visualized with a relatively higher resolution (<40 m) in two or three dimensions. The inner seismic facies can be mapped and help to investigate various volcano-sedimentary processes (Davies et al. 2002; Hansen 2006; Jackson 2012).

Strong impedance contrast exists between igneous rocks and sedimentary rocks. Igneous rocks, particularly mafic rocks, generally display high amplitude at the crest and chaotic facies inside. Given the uncertainty in seismic interpretation, a typical profile (Fig. 3A) in the northern East China Sea Shelf basin, calibrated against borehole data, was used as a reference for this study (Lee et al. 2006). The well E-1 penetrated the crest of a vertical intrusive structure in the profile, manifesting as a conical and massive blanketing zone with a strong crest and chaotic or transparent seismic facies inside the structure. The intrusion had clearly disturbed the stratigraphic structure leading to slight uplift of the surrounding sediments, and those located above the crest of the intrusion. Steeply-dipping strata terminate against the flanks of the intrusion, and overlying layers arch over the crest. These manifestations are typical seismic characteristics of igneous rocks and are used in this study as interpretation criteria to identify such rocks.

Seismic sequences

Twelve seismic horizons have been identified in the Cenozoic strata (Fig. 4), S65.5, S53.5, S32, S30, S23.3, S18.5, S15.5, S13.5, S10.5, S5.5, S2.6 and the seafloor (0 Ma), and verified against biostratigraphy from the nearby industrial borehole BY7-1-1 and academic borehole ODP 1148 (Wang et al. 2000). This dataset enables us to study the characteristics of igneous rocks in detail.

The seismic sequences bounded by the horizons have been named according to two different naming systems in the QDNB and the PRMB, due to historical reasons. The two regions have undergone a range of different tectonic events. Seven important horizons are introduced as follows: (1) S63.5 and S53.5 mark the top of the basement of the PRMB and the QDNB, respectively, and indicate the initiation of continental rifting, corresponding to the Shenhu Event; (2) S32 marks the initiation of seafloor spreading, corresponding to the Nanhai Event. Regional angular unconformities with the underlying strata developed at this time; (3) S23.3 formed as a result of the Baiyun Event, when spreading in the SCS jumped southward and strong subsidence occurred in the Baiyun Sag in the PRMB. This horizon marks the transitional surface between the syn-rift and post-rift stage (Wei et al. 2001). The underlying syn-rift deposition was controlled by early syn-rift faulting, while the overlying post-rift deposition underwent seafloor spreading and was exposed to the resulting thermal subsidence; (4) S15.5 marks the end of seafloor spreading in the SCS. Chaotic seismic reflections are recorded in localized areas near this horizon, probable indication of igneous rocks; (5) S10.5 corresponds to the shelf-slope unconformity in the QDNB, while the sediments show conformity in the PRMB; (6) S5.5 marks the beginning of the neo-tectonics period, corresponding to the Dongsha Event and the Taiwan Orogeny in the northeastern margin of the SCS. These events are associated with block rotation, slight folding, erosion, frequent magmatic activity and angular unconformities.

Seismic characteristics of the igneous rock structure

Combining the identification criteria outlined above and their geometric appearance, the igneous rocks of the deep water basins in the northern SCS can be investigated and distinguished with regard to their extrusive or intrusive nature.

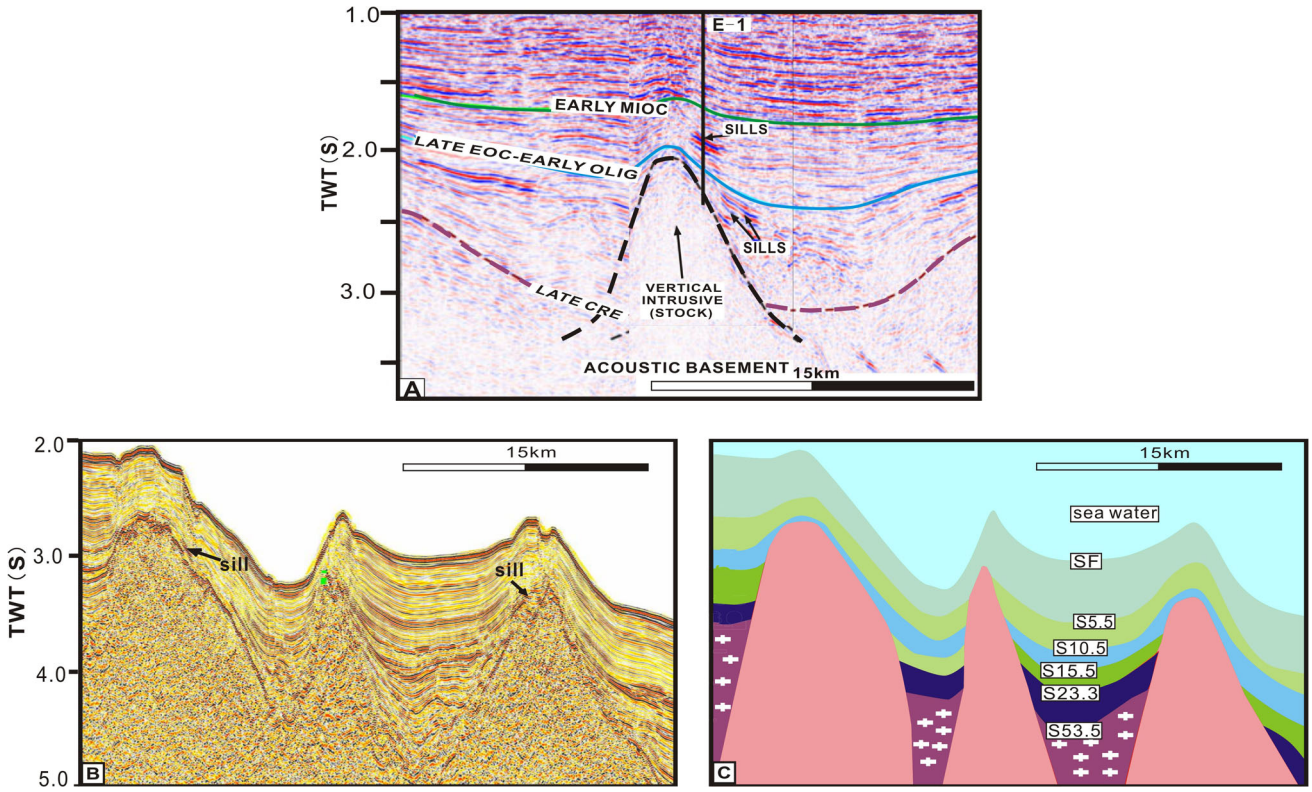

Fig. 3 Seismic profile of the northern East China Sea Shelf Basin showing a vertical intrusion (**A**) and the typical magmatic structures in the northern SCS (**B**, **C**). The vertical intrusion in (**A**) appears to have uplifted the overburden and upturned the host rocks (modified after Deniz et al. 2010). Location of the seismic section displayed in B is shown in Fig. 2. *White plus* represents crystalline basement

Extrusive structures

In seismic profiles, extrusive structures form seamounts and buried volcanoes. Seamounts distributed in the northern margin of the SCS can be further classified into two types based on morphology: flat-topped seamounts and conical-topped seamounts.

A typical flat-topped seamount is characterized by a flat and broad top, but a steep slope (Fig. 5). The ratio between the width of the flat top and the height of the slope above the seafloor is approximately 1:1. Generally, sedimentary layers develop on the top of this type of seamount. The strata gradually thin from the center to the edge of the flat-topped platform with increasing slope, and pinch out at the junction of the platform and the slope. A higher magnetic anomaly can be observed across Fig. 5, suggesting that the seamount might be of basaltic nature rather than continental crust or a shallow water sandstone deposits (Fig. 5).

The conical-topped seamounts are suggested to be formed by the strong central eruption of a volcano (Planke et al. 2000). Clear magmatic conduits can be recognized in this type of seamount (Fig. 6). In contrast with flat-topped seamounts, the conical-topped seamounts have a high and sharp head which is exposed above seafloor. The ratio between the width of the conical top and the height of the seamount is roughly 1:6. The size and shape of conical-topped seamounts varies greatly according to the eruption energy. The volcanic eruption leads to disordered internal reflections in the seamount and uplift and steeply dipping adjacent strata (Fig. 6). We speculate that this phenomenon is associated with violent and rapid eruptions. Compared with flat-topped seamounts, conical-topped seamounts are likely to be relatively recent structures, as the conical top implies the absence of long term erosion. There are 55 conical-topped seamounts across the entire northern margin of the SCS, making them the dominant type of extrusive structure in this area. They are predominantly distributed along faults.

Intrusive volcanic structures

Intrusive structures can be further divided into piercement and implicit-piercement types, based on the intrusive energy. Igneous intrusions can form concentric folds in the overlying strata (Fig. 3B), with obvious uplift of the strata at the flanks. The seismic characteristics of these structures are: internal chaotic, high frequency and low amplitude seismic facies. Compared with the implicit-piercement

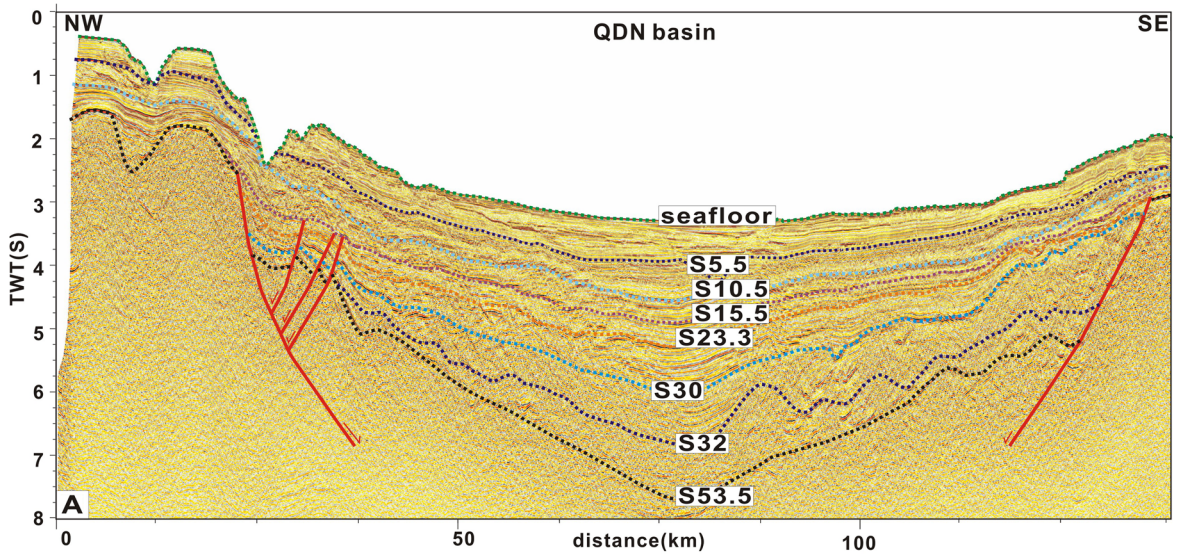
NW
QDN basin
SE
TWT(S)
seafloor
S5.5
S10.5
S15.5
S23.3
S30
S32
S53.5
A
distance(km)
0
50
100

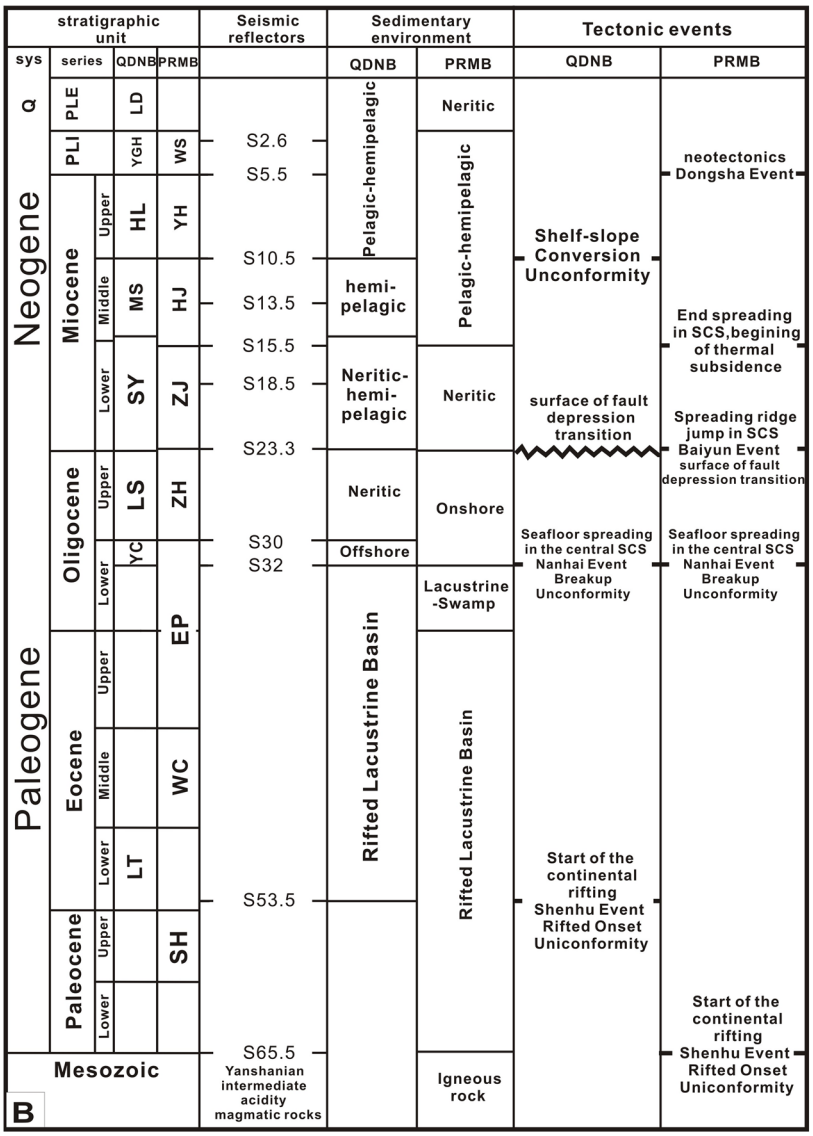
stratigraphic unit
Seismic reflectors
Sedimentary environment
Tectonic events
sys
series
QDNB
PRMB
QDNB
PRMB
QDNB
PRMB
Q
Neogene
Paleogene
Mesozoic
PLE
PLI
Miocene
Oligocene
Eocene
Paleocene
Upper
Middle
Lower
LD
YGH
HL
MS
SY
LS
YC
LT
WS
YH
HJ
ZJ
ZH
EP
WC
SH
S2.6
S5.5
S10.5
S13.5
S15.5
S18.5
S23.3
S30
S32
S53.5
S65.5
Yanshanian intermediate acidity magmatic rocks
Pelagic-hemipelagic
Neritic
Pelagic-hemipelagic
hemi-pelagic
Neritic-hemi-pelagic
Neritic
Neritic
Onshore
Offshore
Lacustrine -Swamp
Rifted Lacustrine Basin
Rifted Lacustrine Basin
Igneous rock
Shelf-slope Conversion Unconformity
surface of fault depression transition
Seafloor spreading in the central SCS Nanhai Event Breakup Unconformity
Start of the continental rifting Shenhu Event Rifted Onset Uniconformity
neotectonics Dongsha Event
End spreading in SCS,begining of thermal subsidence
Spreading ridge jump in SCS Baiyun Event
surface of fault depression transition
Seafloor spreading in the central SCS Nanhai Event Breakup Unconformity
Start of the continental rifting Shenhu Event Rifted Onset Uniconformity
B

◀**Fig. 4** Seismic profile crossing the Qiongdongnan basin (**A**) and Stratigraphic table with sequences, unconformities and major tectonic events affecting the South China Sea (**B**; after Wang et al. 2013a, b; Sun et al. 2013). Location of the seismic section displayed in (**A**) is shown in Fig. 2. *Q* Quaternary, *PLE* Pleistocene, *PLI* Pliocene, *LD* Ledong, *YGH* Yinggehai, *WS* Wanshan, *HL* Huangliu, *YH* Yuehai, *MS* Meishan, *HJ* Hanjiang, *SY* Sanya, *ZJ* Zhujiang, *LS* Lingshui, *ZH* Zhuhai, *YC* Yacheng, *EP* Enping, *WC* Wenchang, *SH* Shenhu, *LT* Lingtou

type intrusion which will be introduced below, the piercement-type intrusion usually indicates higher energy. The energy of magma intrusion is so strong that it can reach the ultimate fracture strength of the overlying strata, but is not able to pierce all the overlying strata. Therefore, many small-scale normal faults often develop at the top of intrusive structures.

There is a special piercement type intrusive rock in the study area, characterized by a star-shaped head and chaotic internal reflection (Fig. 7). These structures are distributed widely in the Xisha area. Most of the star-shaped heads are found in the Yinggehai Formation, and partially in the Huangliu Formation, clearly indicating that they developed later than these formations. We speculate the formation of these structures involves a rapid intrusion, in which the magma intrudes vertically upward into the sedimentary layers in such a very short period of time, that there is no significant uplift on both sides of the adjacent strata. There are 22 intrusive structures with star-shaped head in the study area, mostly distributed in the eastern Xisha area and the western PRMB.

In contrast to the piercement type structure, the implicit-piercement structure has weaker magmatic energy, evidenced by the extensive gentle fluctuation of the overlying strata, especially the top of the basement. Inside the intrusion, the seismic facies are high amplitude chaotic. The interface between the intrusion and the overlying strata also show strong continuity.

Differences between intrusions and buried volcanoes

A buried volcano refers to a volcano that previously erupted above the seafloor, and was subsequently covered by sediments. Generally, the seismic characteristics of piercement type intrusions are similar to that of buried volcanoes. The main differences between intrusive structures and buried volcanoes in the seismic profiles are (1) the overlying strata above intrusive rocks are arched with a similar deflection to the intrusive crest (Fig. 8C, D) induced by the doming effect of the intrusion; (2) as for the contact relationship between the strata and the igneous rock, obvious angular unconformities can be found at the volcano-sediment interface (Fig. 8A, B), but a conformable

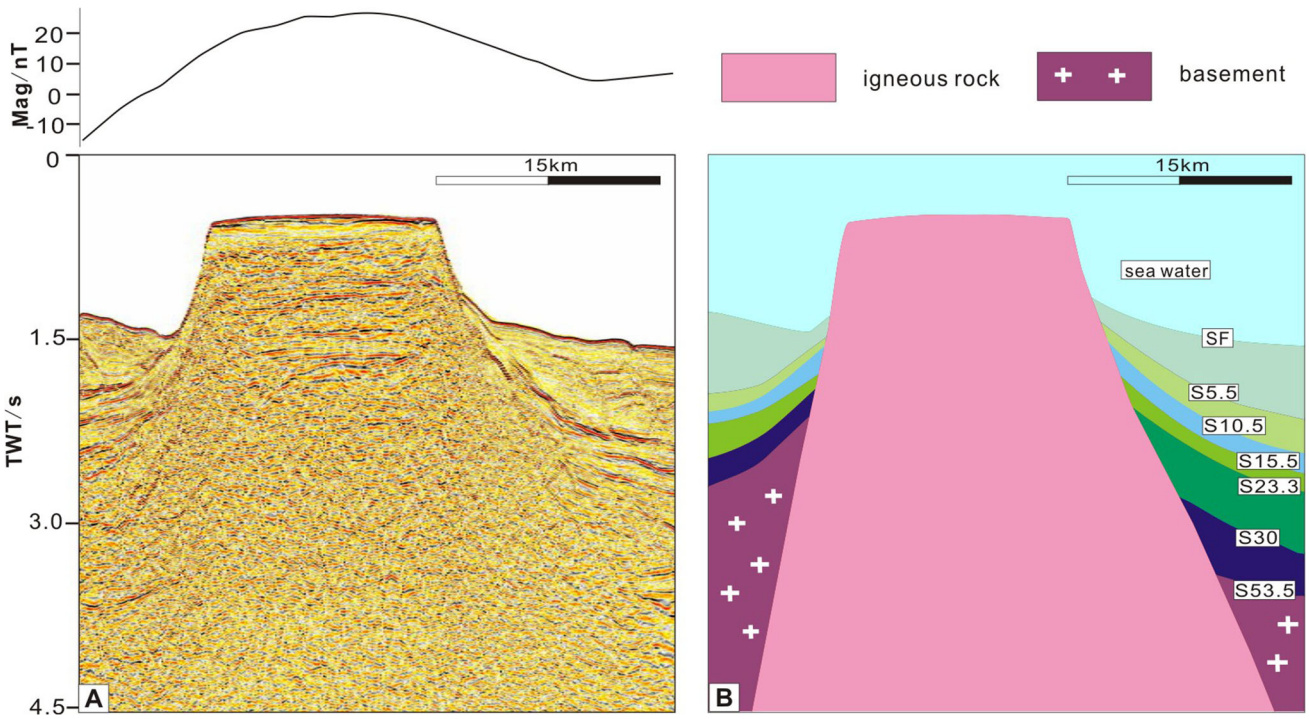

Fig. 5 Seismic profile (**A**) and its schematic illustration (**B**) of a flat-topped seamount in the northern SCS. Magnetic anomaly along this profile is shown. Location of the seismic section displayed in (**A**) is shown in Fig. 2

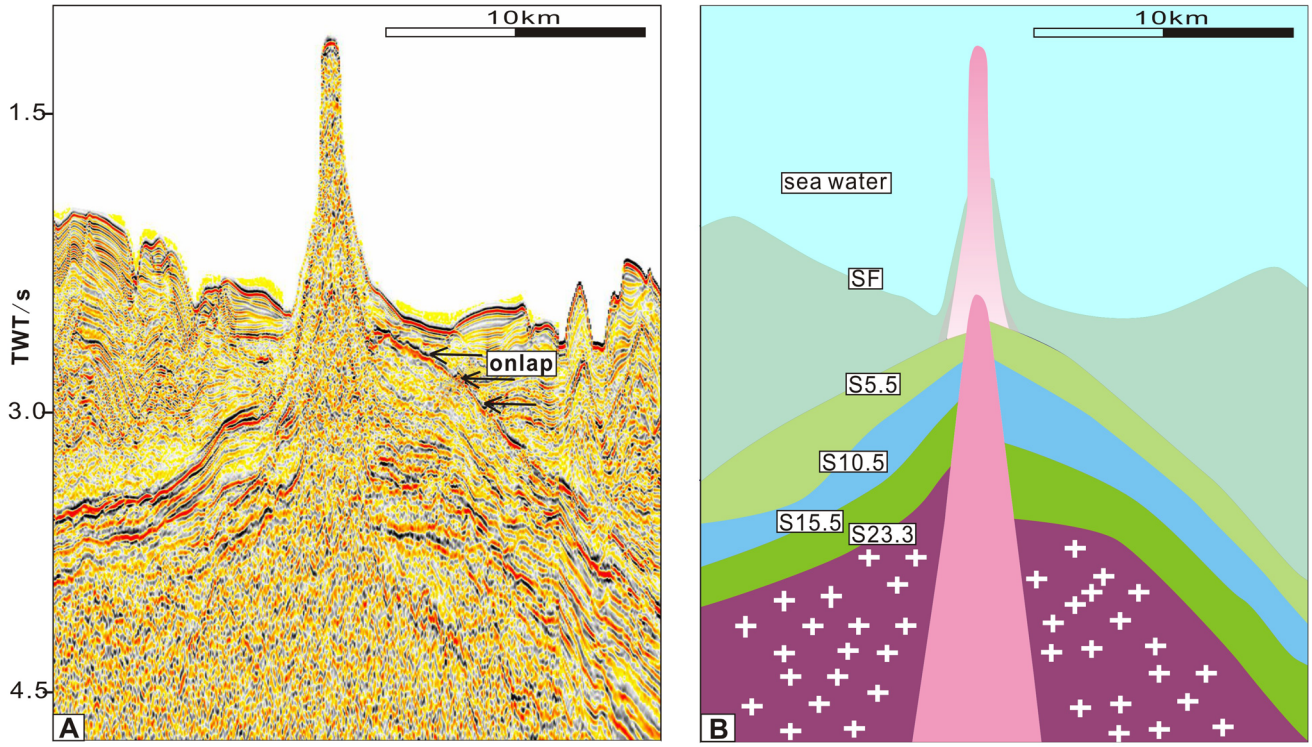

Fig. 6 Seismic profile (**A**) and its schematic illustration (**B**) of a conical-topped seamount. Location of the seismic section displayed in (**A**) is shown in Fig. 2. Legend is the same as that in Fig. 5

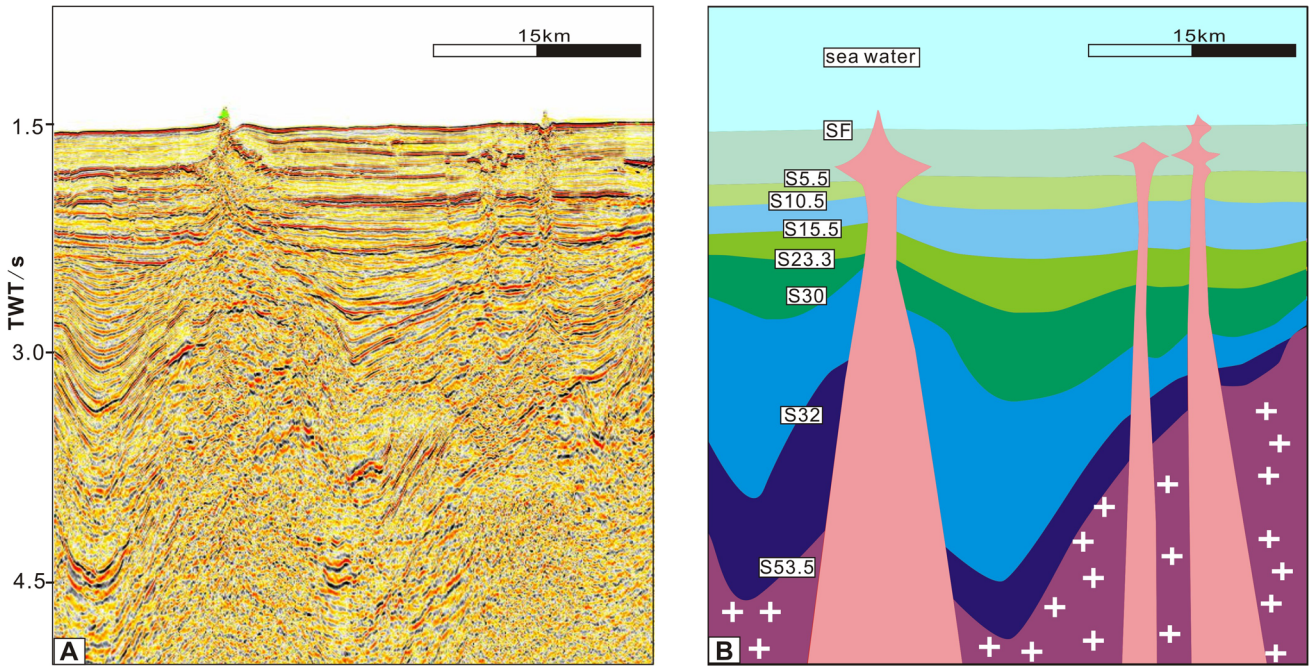

Fig. 7 Seismic profile (**A**) and its schematic illustration (**B**) of a star-shaped head intrusive rock. Location of the seismic section displayed in (**A**) is shown in Fig. 2. The legend is the same as that in Fig. 5

contact usually develops at the intrusion-sediment interface; and finally; (3) intrusions generally form at a relatively slow pace in comparision to the formation of a volcano, and thus sills can usually be found on the top and/or in the surrounding area of the intrusive structure (Figs. 3B, 8C).

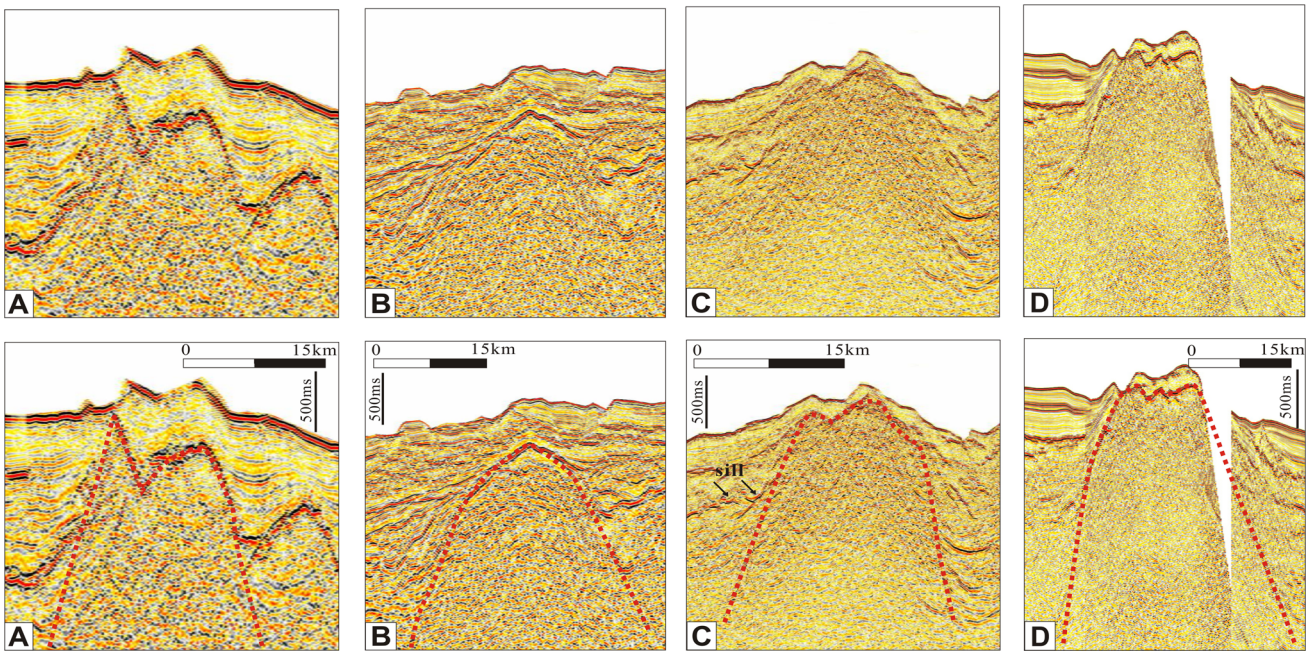

Fig. 8 Seismic profiles showing buried volcanoes (**A**, **B**) and intrusive structures (**C**, **D**). Location of the seismic section displayed in (**A**, **B**, **C**, **D**) is shown in Fig. 2

Timing of igneous rock formation

Seismic characteristics contain chronological information pertaining to specific events and can be used to determine the approximate formation time of igneous bodies, although there is still controversy surrounding this method of determination using seismic data. The timing of igneous rock formation can be determined by identifying and dating the onlap of intrusion-related forced folds onto the flanks of of the intrusion (Trude et al. 2003; Svensen et al. 2004; Hansen et al. 2008). The contact relationship, sedimentary thickness and seismic reflection contrast are the three criteria used in this study to estimate the formation time of igneous rocks.

Contact relationship

The most obvious feature in the contact relationship between igneous structures and the surrounding strata is angular unconformity. The igneous structures are covered by overlying strata, which are uplifted as a result of the intrusion. The strata deposited after magma intrusion generally form distinct angular unconformities on the flanks of the intrusion-related forced folds. The section shown in Fig. 9 (ii′ in Fig. 2) illustrates that uplift occurs in the strata adjacent to the igneous rock, below horizon S15.5, indicating that this event was triggered by magmatism that occurred at least 15.5 Ma. Further analysis reveals that the strata between S10.5 and S15.5 were also uplifted by the intrusion, while the overlying strata above S10.5 developed obvious on-lap features above the uplifted S10.5, and were apparently unaffected by the magmatism. Consequently, this igneous event could be estimated to have taken place at approximately 10.5 Ma.

Sedimentary thickness

The seismic profile in Fig. 10 is located in the Xisha uplift. The strata overlying igneous structures are relatively thin on top of these structures and thick at their flanks (Fig. 10). The influence of differential compaction indicates that the igneous rocks formed before deposition of the Meishan Formation. Therefore, the occurrence of thickness variations in intrusion-related forced folds can be applied to evaluate the timing of magmatism.

In contrast to Fig. 10, the seismic section in Fig. 9 displays a different thickness pattern of the overlying strata. The Meishan Formation (Fig. 9) is relatively uniform in thickness both on top and in the flanks of the igneous structure. This indicates that the magmatism occurred after the deposition of Meishan Formation, at least 10.5 Ma ago.

Seismic reflection contrast

Under certain conditions, strata might have contrasting characteristics on either side of an igneous structure that can point to the timing of rock formation. This is

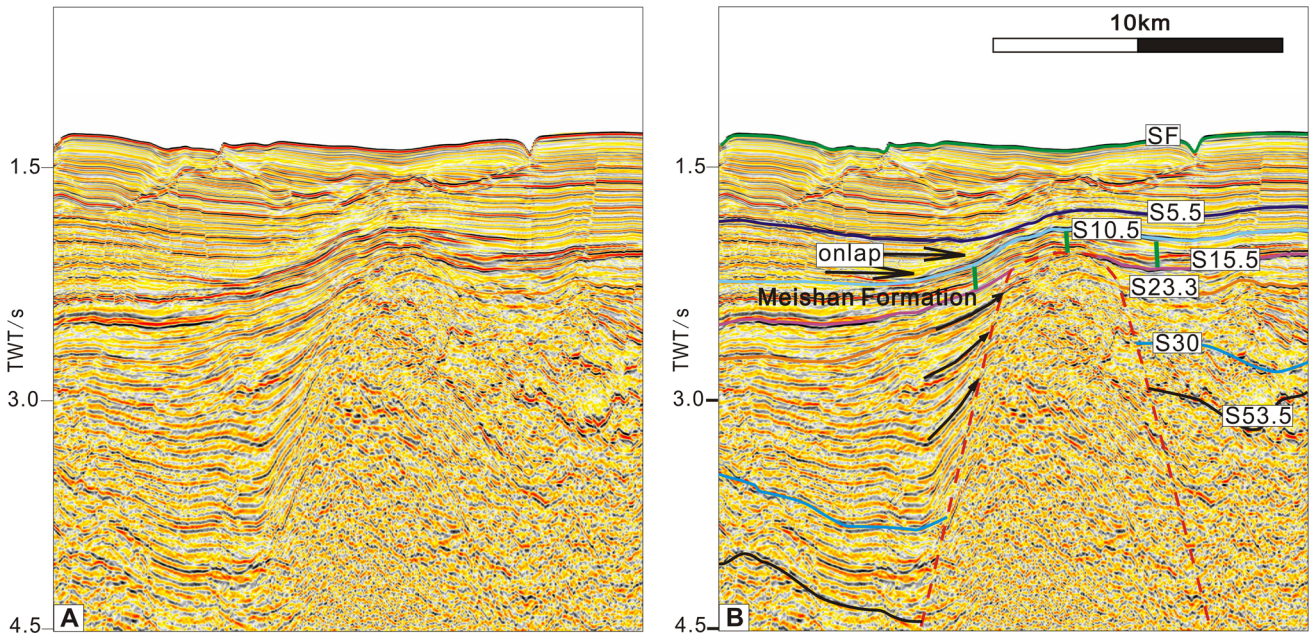

Fig. 9 Seismic profile (**A**) and its schematic illustration (**B**). Location of the seismic section displayed in (**A**) is shown in Fig. 2

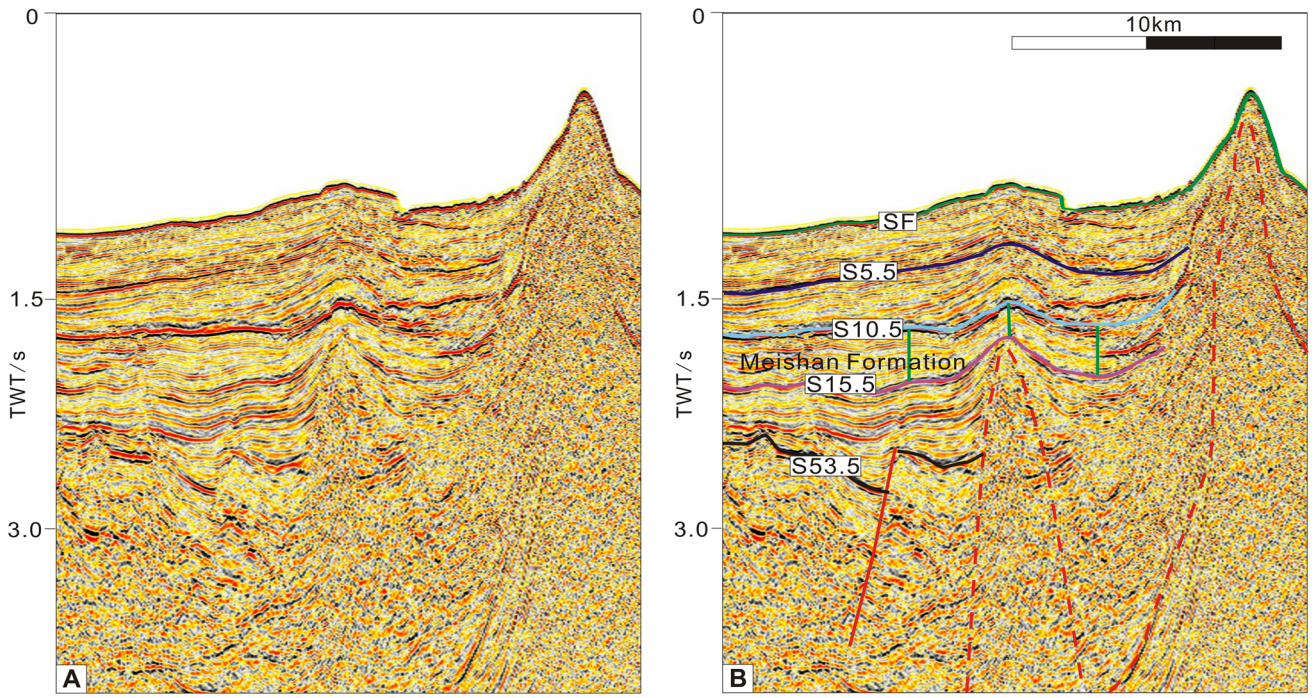

Fig. 10 Seismic profile (**A**) and its schematic illustration (**B**). Location of the seismic section displayed in (**A**) is shown in Fig. 2

particularly the case for structures close to the continental shelf or slope that have a sediment source mainly coming from the continental margin. If a volcano formed at an earlier time, it would have obstructed sediment transport, resulting in different seismic characteristics in the strata on both sides of the structure. In this case, it is difficult to evaluate the timing of igneous rock formation using the contact relationship and sedimentary thickness. Contrasting seismic reflections on both sides of the igneous structure may be an alternative method to determine the timing of the igneous event. When the seismic reflections are alike, it is suggested that the igneous event may have taken place after the deposition of the punctured strata, and vice versa (Figs. 6, 11).

The volcanoes of the northwestern subbasin (Fig. 11) experienced no uplift in the strata adjacent to the flanks of the igneous structure. We therefore estimate that the volcanoes formed prior to sediment deposition. Most of the sediment in this area originates from vertical deposition in the oceanic basin, leading to no difference in the seismic characteristics of the sediments on either flank of the structure. The timing of volcano formation therefore corresponds to onset of the seafloor spreading in the Northwestern basin.

These age estimations, based on seismic profiles, are evaluated and verified by comparison against radioactively dated extrusive seamounts. Although the seismic profiles, studied herein, do not capture these extrusive seamounts, they are located very close to or surrounded by our seismic data. We can see from Fig. 15A, seamount 1 is located at S04-12, near the Zhongsha uplift. According to our seismic data surrounding seamount 1, this seamount is younger than 5.5 Ma (orange areas in Fig. 15A), while radioactive dating indicates that this seamount is younger than 5.5 Ma (Table 1). Therefore, it is consistent with our results. Seamounts 2, 3 are Late Miocene-Recent igneous rocks (Yan et al. 2006) located in the NW Subbasin and the SCS basin respectively. They are close or surrounded by igneous rocks after 5.5 Ma (orange areas in Fig. 15A). This is also consistent with our results from seismic age dating.

Stratal architecture in relationship to extrusive and intrusive structures in the northern SCS

Large scale extrusive structures generally cause high angle uplift in the adjacent sedimentary rocks. The strata deposited after extrusion are usually horizontal or slightly upward-sloping against the flanks of the igneous structure. An on-lap boundary exists between the strata formed

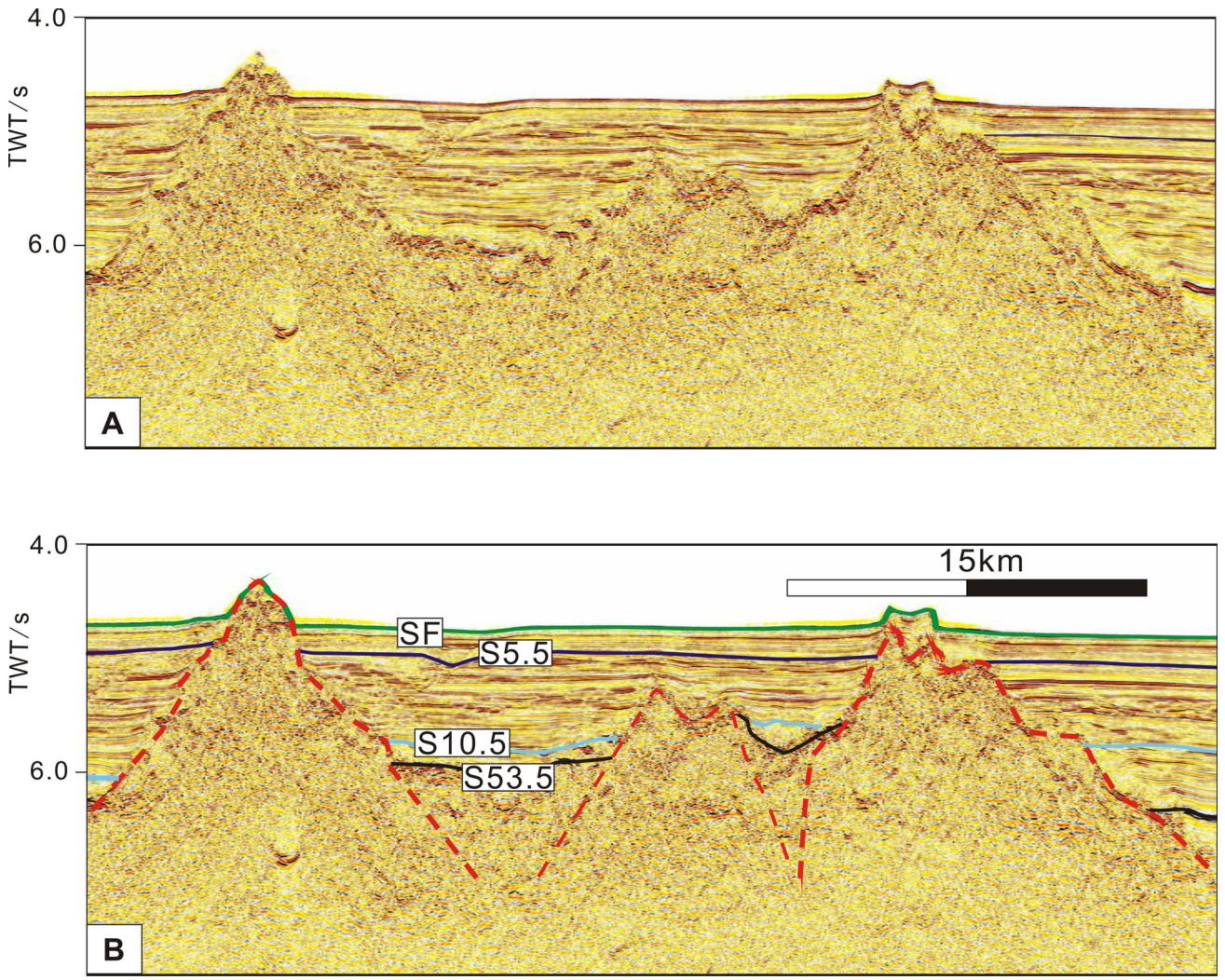

Fig. 11 Seismic profile (**A**) and its schematic illustration (**B**). Location of the seismic section displayed in (**A**) is shown in Fig. 2

Table 1 Chronological history of igneous rocks of the SCS and surrounding areas, as reviewed from the existing literature

Station	Lon. (°E)	Lat. (°N)	Age (Ma)	Area	Source
V36D10	115.6	14	3.49	Nansha	Taylor and Hayes (1983)
D1	111.97	13.37	0.4	Nansha	Zhou et al. (2005)
D3	111.17	9.95	4.3	Nansha	Zhou et al. (2005)
1143	113.28	9.36	<2	Southern margin	Wang et al. (2000)
D3	111.17	9.95	4.3	Southern margin	Bellon and Rangin (1991)
SO23-37	116.62	12.08	0.4	Southern margin	Kudrass et al. (1986)
SO23-38	118.3	11.73	0.5	Southern margin	Kudrass et al. (1986)
SO23-40	118.82	12.35	2.7	Southern margin	Kudrass et al. (1986)
SO23-15	119.37	8.17	14.7	Southern margin	Kudrass et al. (1986)
SO23-23	115.87	9.9	T3-J1(?)	Southern margin	Kudrass et al. (1986)
SO23-24	115.83	9.88	T2(?)	Southern margin	Kudrass et al. (1986)
YJ21-1-1	112.3	20.45	51.6 ± 8.3	PRMB	Rao and Li (1991)
711	114	19.65	17.1 ± 2.5	PRMB	Zou et al. (1995)
BY7-1-1	114	19.65	17.6 ± 1.8	PRMB	Rao and Li (1991)
BY7-1-1	114	19.65	35.5 ± 2.8	PRMB	Rao and Li (1991)
P1611	114.85	20.48	41.2 ± 2.0	PRMB	Zou et al. (1995)
3321	114.3	21.1	24.3 ± 1.3	PRMB	Zou et al. (1995)
L1112	115.8	20.77	27.2 ± 0.6	PRMB	Zou et al. (1995)
L411	115.5	20.85	43.2 ± 0.7	PRMB	Zou et al. (1995)
H2111	115.31	21.32	41.1 ± 0.7	PRMB	Zou et al. (1995)
HZ27-1-1	115.4	21.26	57.1 ± 2.5	PRMB	Rao and Li (1991)
L111	116.05	21.9	32 ± 1.4	PRMB	Zou et al. (1995)
L111	116.05	21.9	33.6 ± 0.7	PRMB	Zou et al. (1995)
L1511	116.49	21.46	45.1 ± 1.6	PRMB	Zou et al. (1995)
1148	116.57	18.84	<1	PRMB	Wang and Chen (1999)
LH4-1-1	115.55	19.84	43.2 ± 0.7	PRMB	Rao and Li (1991)
WSH-2	109.13	21.05	5.9 ± 1.2	Weizhou island	Jia et al. (2003)
SK-1	109.6	21.7	2.4 ± 0.1	Weizhou island	Jia et al. (2003)
PB-2	103.69	22.99	1.1 ± 0.1	Weizhou island	Jia et al. (2003)
YL-7	109.97	22.28	99.8 ± 2.4	Weizhou island	Jia et al. (2003)
TW36	121.483	22.666	1.9	Taiwan segment	McDermott et al. (1993)
TW40	121.483	22.666	2.9	Taiwan segment	McDermott et al. (1993)
Ca2	122.1541	18.214	1.27	Philippines	McDermott et al. (1993)
Ca11	122.1541	18.214	0.32 ± 0.05	Philippines	McDermott et al. (1993)
Ca9	122.1541	18.214	0.64 ± 0.19	Philippines	McDermott et al. (1993)
47A	120.596	16.4023	2.9	Luzon segment	McDermott et al. (1993)
38A	120.596	16.4023	2.8	Luzon segment	McDermott et al. (1993)
PL41	120.596	16.4023	0.8	Luzon segment	McDermott et al. (1993)
B5	121.936	20.371	0.01	Philippines	McDermott et al. (1993)
B82	121.936	20.371	0.45 ± 0.13	Philippines	McDermott et al. (1993)
B88	121.936	20.371	0.76 ± 0.04	Philippines	McDermott et al. (1993)
B93	121.936	20.371	1.07 ± 0.16	Philippines	McDermott et al. (1993)
B46	121.936	20.371	2.32	Philippines	McDermott et al. (1993)
B86	121.936	20.371	1.71	Philippines	McDermott et al. (1993)
B80	121.936	20.371	2.96	Philippines	McDermott et al. (1993)
756	108.333	11.5	17.6–7.9	Indochina peninsula	Hoang et al. (1996)
804	107.944	11.25	8–3.4	Indochina peninsula	Hoang et al. (1996)
63	108.038	12.666	5.8–1.67	Indochina peninsula	Hoang et al. (1996)

Table 1 continued

Station	Lon. (°E)	Lat. (°N)	Age (Ma)	Area	Source
121	108	13.983	4.3–0.8	Indochina peninsula	Hoang et al. (1996)
516	107.234	10.932	0.88–0.44	Indochina peninsula	Hoang et al. (1996)
R-2	109.014	10.158	0.8–0	Indochina peninsula	Hoang et al. (1996)
S04-11	116.099	16.343	7.91 ± 0.19	SCS basin	Yan et al. (2008)
S04-12-10	113.159	15.572	4.78 ± 0.11	SCS basin	Yan et al. (2008)
S04-12-11	113.159	15.572	5.74 ± 0.13	SCS basin	Yan et al. (2008)
S04-12-18	113.159	15.572	5.18 ± 0.17	SCS basin	Yan et al. (2008)
S04-12-20	113.159	15.572	4.76 ± 0.12	SCS basin	Yan et al. (2008)
S04-12-21	113.159	15.572	4.94 ± 0.11	SCS basin	Yan et al. (2008)
S04-14-1	115.384	14.039	6.33 ± 0.20	SCS basin	Yan et al. (2008)
S08-69-1	112.534	10.321	3.8 ± 0.1	SCS basin	Yan et al. (2008)
8	116.983	17.617	13.8–14.1	SCS basin	Wang et al. (1984)
9	116.5	14.8	9.5–9.9	SCS basin	Wang et al. (1984)
10	115.583	14	3.49	SCS basin	Wang et al. (1984)
DR01	116.18	15.75	11–6	SCS basin	Pautot et al. (1990)
DR02	115.96	15.3	11–6	SCS basin	Pautot et al. (1990)
DR03	116.21	14.95	8–6	SCS basin	Pautot et al. (1990)
NO.8	116.98	17.75	13.95	SCS basin	Jin (1989)
NO.9	116.52	15	9.7	SCS basin	Jin (1989)

before and after the eruption, as shown in Fig. 12. The shape of the extrusive body may be flat-topped or conical-topped. Before extrusion, the strata on both sides have almost the same thickness; however, the thickness may vary after extrusion, depending on the sedimentation patterns. When the volcano is located in an oceanic basin, the thickness of the strata on both sides will be the same, dominated by vertically-deposited sediments. However, if the volcano is located in the continental shelf or slope, the thickness of strata deposited on the continental side of the volcano will be thicker than that strata deposited on the ocean side of the volcano, resulting from higher sediment supply from the continental margin.

Regarding intrusive structures, both large and small scale structures have been found in the study area. In large-scale intrusive structures, the pierced strata show obvious uplift, while the overlying strata are uplifted in a similar manner to that of the underlying intrusive rock. The strata deposited after intrusion are gently uplifted or show a slight angular unconformity with the underlying strata. As for small scale intrusive structures, the magma conduit can easily be identified. The lower sedimentary strata are pulled up at a relatively small angle and have the same thickness on both sides of the intrusion. The intrusive structures have a diverse shape, such as mushroom, tower, door, star etc. A conformable surface or a very slight angular unconformity exists at the contact between the strata deposited before and after the intrusion.

As an example, the large scale intrusive structure of Fig. 13 pierced and pulled up the lower sedimentary strata. The dip of the strata changes dramatically above and below horizon S5.5. The overlying strata are uplifted and form a conformable contact with the underlying strata. Therefore, the timing of this intrusion is suggested to be at least 5.5 Ma.

Discussion

Sedimentation processes on flat-topped seamounts

Sediments are often found on top of extrusive structures, especially flat-topped seamounts. Two processes may be used to explain their deposition. One is that most of the flat-topped seamounts were ancient volcanoes which subsequently sunk. If the depth of the magma eruption was higher than the pressure compensation depth (PCL), explosive volcanism could occur and produce volcaniclastic sediments (e.g., Yan and Shi 2009). Volcanic eruptions could become explosive due to interaction of wet sediments and magma, forming internally chaotic volcanic-sedimentary complexes at the top. Subsequently, long-term

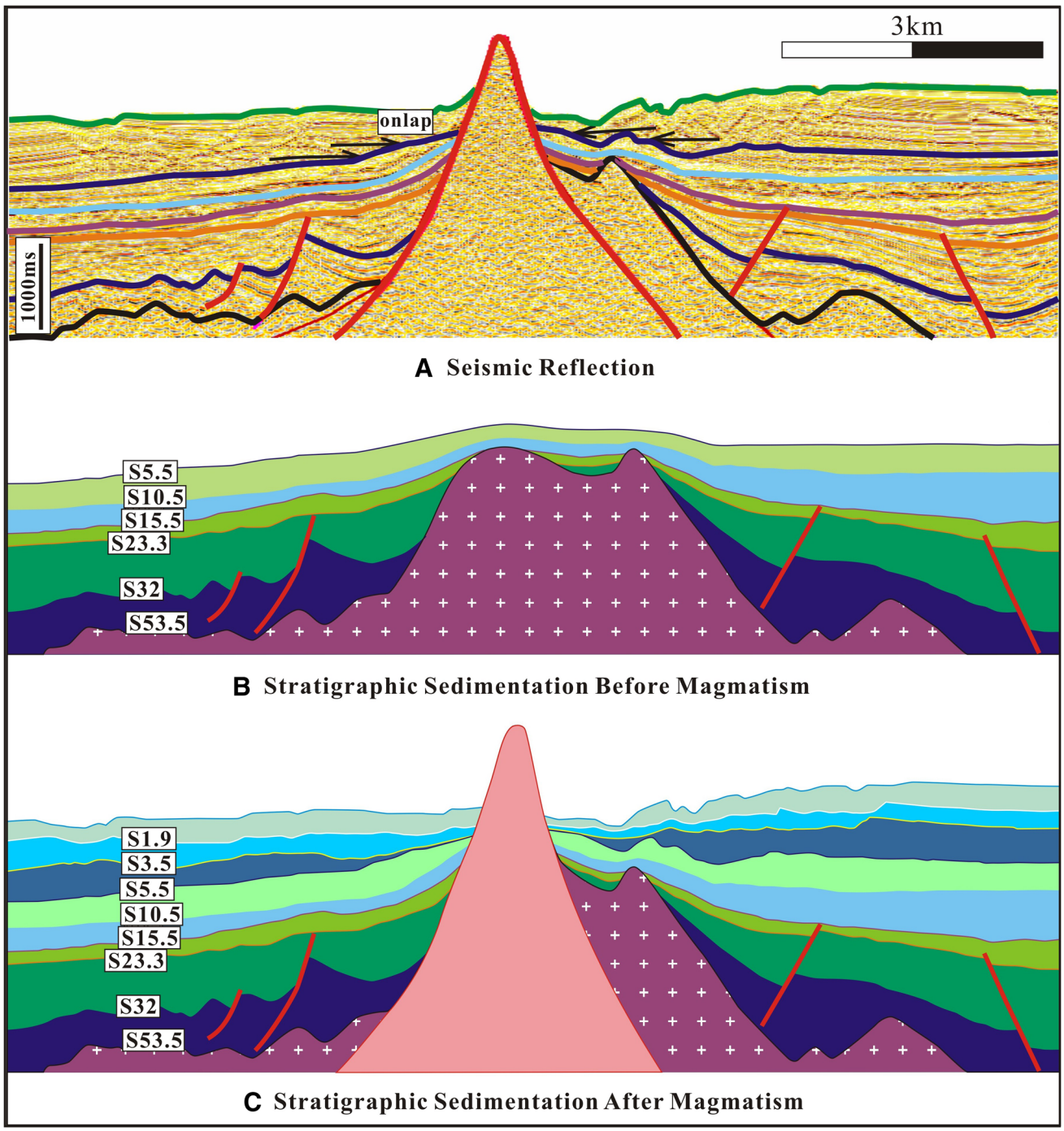

Fig. 12 Seismic profile over large scale extrusive structure (**A**); **B**, **C** stratigraphic architecture before and after magmatism. Location of the seismic section displayed in (**A**) is shown in Fig. 2

erosion would eventually shape the flat top of the volcano. Another possibility is that the flat-topped seamount was a crater colonized by corals near sea level. A large number of dead corals would have accumulated in the centre of crater, which led to an atoll with a flattened top. Shallow-water carbonates may then have been deposited, evolving into huge, flat-topped seamounts (Zhang et al. 2007).

Distribution of igneous rocks in the northern margin of the SCS

Based on boreholes of the PRMB in the northern SCS, Zou et al. (1995) revealed the relationship between igneous rocks and its surrounding strata and combined his observations with isotope dating data. Zou et al. (1995) divided

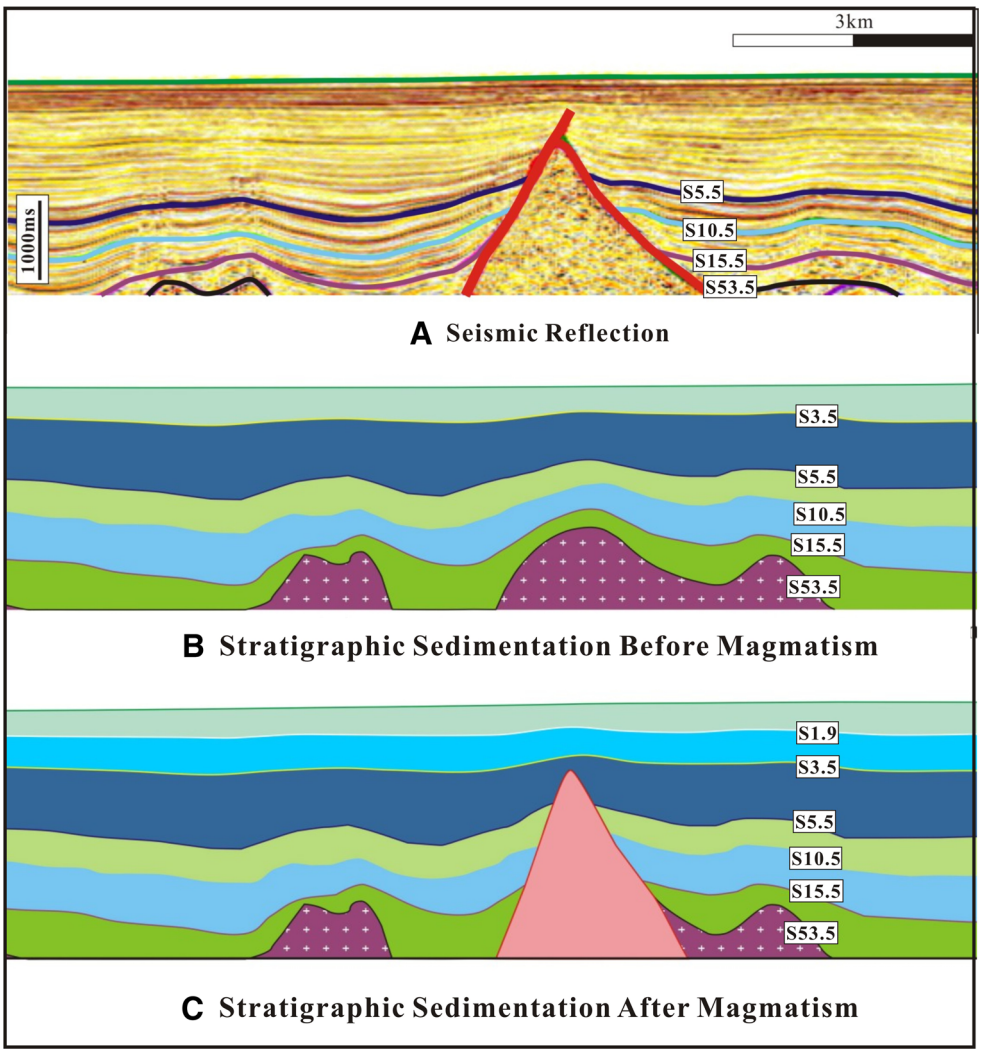

Fig. 13 Seismic profile over large scale intrusive structure (**A**); **B**, **C** stratigraphic architecture before and after magmatism. Location of the seismic section displayed in (**A**) is shown in Fig. 2

Cenozoic magmatism into eight periods: Paleocene, Eocene, Oligocene, Early Miocene, Middle Miocene, Late Miocene, Pliocene and Quaternary (Fig. 14).

We divide the Cenozoic magmatism of the study area into the three periods based on their seismic characteristics (Fig. 15A): before seafloor spreading (Paleocene and Eocene), during seafloor spreading (Early Oligocene–Mid Miocene) and after seafloor spreading (Mid Miocene–Recent), respectively. Almost all Cenozoic igneous rocks are concentrated below the 1500 m bathymetric contour. The distribution of igneous rocks is also supported by magnetic anomalies, which suggests that the major Cenozoic igneous rocks in the northern margin of the SCS are highly consistent with a high-value magnetic anomaly zone (Fig. 15B). As shown in Fig. 15B, the highest magnetic anomaly, approximately 100nT, is located near the NW Subbasin.

Paleocene and Eocene (before seafloor spreading; Fig. 16A): During the rifting and before seafloor spreading, igneous rocks were sporadically emplaced in the southern part of the Dongsha uplift and the NW subbasin, and could not be found in the Xisha areas in seismic reflection profiles, possibly because the rifting stage propagated from east to west, and the subsequent stronger extension of the eastern SCS compared to the western SCS. Igneous rocks did not form in the northwestern margin of the SCS at this time, which is consistent with the period of magmatic quiescence in the Paleogene. Small-scale magmatism occurred during this period in the eastern coastal rifted basin (Zhou and Li 2000). The dispersed Cenozoic magmatism over the SCS margins differed greatly from the large igneous provinces in volcanic margins, where mantle plumes had played a significant role in facilitating or driving continental rifting and breakup. However, no evidence of surface igneous rocks indicates the presence of a mantle plume since rifting initiated in the study area (Flower et al. 1998).

Early Oligocene to Mid Miocene (during seafloor spreading; Fig. 16B) Magmatism increased intensively

during the Eocene but was still limited in extent and generally distributed on the continental slopes, such as the southwestern part of the northeastern SCS and the Xisha areas. Igneous rock formation was important and mainly distributed along the fault junction surrounding the Xisha and Zhongsha uplift (Fig. 16B). Although the level of activity during seafloor spreading remains controversial, we propose that magmatism was active in the northern margin of the SCS. Using the criteria mentioned above, we have identified the magmatism related to seafloor spreading of the SCS (Fig. 14) from the sedimentary sequence deposited between S30 and S15.5. These sediments have been pulled up by intrusions, while the overlying strata did not record any obvious influence from these intrusions. We suggest that magmatism was quite active for the period characterized by seafloor spreading in the SCS, as opposed to Yan et al. (2006). Additional evidence to support increased magmatic activity during this time includes nine layers of lower Miocene alkaline basalt and basaltic tuff lava that were found in the well BY7-1-1 in the PRMB. Their K–Ar age is 17.1 ± 2.5 and 20.2 ± 3.0 Ma, for the levels at 2429 and 2432 m, respectively (Zou et al. 1995). Furthermore, one seamount, located in the northern margin of the SCS, was dated to 18.61 ± 4.89 Ma using the K–Ar dating method too (Li et al. 1991).

Lithological evidence and seismic tomography suggest that the Hainan plume, which has a deep mantle origin is beneath the Hainan Island (Hart et al. 1992; Hauri et al. 1994; Lebedev et al. 2000; Lebedev and Nolet 2003; Yan and Shi 2007; Zou and Fan 2010; Campbell and O'Neill 2012; Wang et al. 2013a, b; Montelli et al. 2006). The plume-induced magmatism started at ca. 30 Ma (Yeh et al. 2010), which implies that the head of the Hainan plume likely impinged on the base of the lithosphere during seafloor spreading (Wang et al. 2013a, b; Ho et al. 2000).

Fig. 15 **A** Distribution of three periods of magmatism in the northern SCS margin. Magmatism is most active since 5.5 Ma. **B** Magnetic anomalies map with the distribution of igneous rocks (*black areas*). Several igneous rocks shown in previous figures (Figs. 5, 7, 10, 11, 14) are *marked*

Mid-Miocene to Recent (after seafloor spreading; Fig. 16C, D) Magmatism during this last period is widely distributed and further divided into two stages with different scales. The first stage dates from 15.5 to 5.5 Ma (Fig. 17C), after the cessation of seafloor spreading and prior to neo-tectonic activity. This stage is characterized by a few small igneous structures, scattered in the Xisha uplift and the NW subbasin. Conversely, the second stage of magmatism, which began at 5.5 Ma, and the igneous structures associated with this stage were distributed all over the study area (Fig. 16D). Individual igneous structures associated with this stage are smaller in the western area than in the eastern area. Igneous rocks are mainly concentrated along deep-faults or in areas surrounded by several faults (Fig. 16D). A great number of igneous rocks erupted again after seafloor spreading (Fig. 6). Magma in the former conduit or magma chamber led to new extensive magmatism since 5.5 Ma. The igneous structures mainly strike ENE-WSW in the PRMB, mostly in the lower slope. We speculate that these widely distributed igneous rocks are closely related to the Dongsha event. The magma was underplated beneath the bottom of the lower crust and formed a high velocity layer which altered the isostasy of the crust. This resulted in uplift of the upper crust and

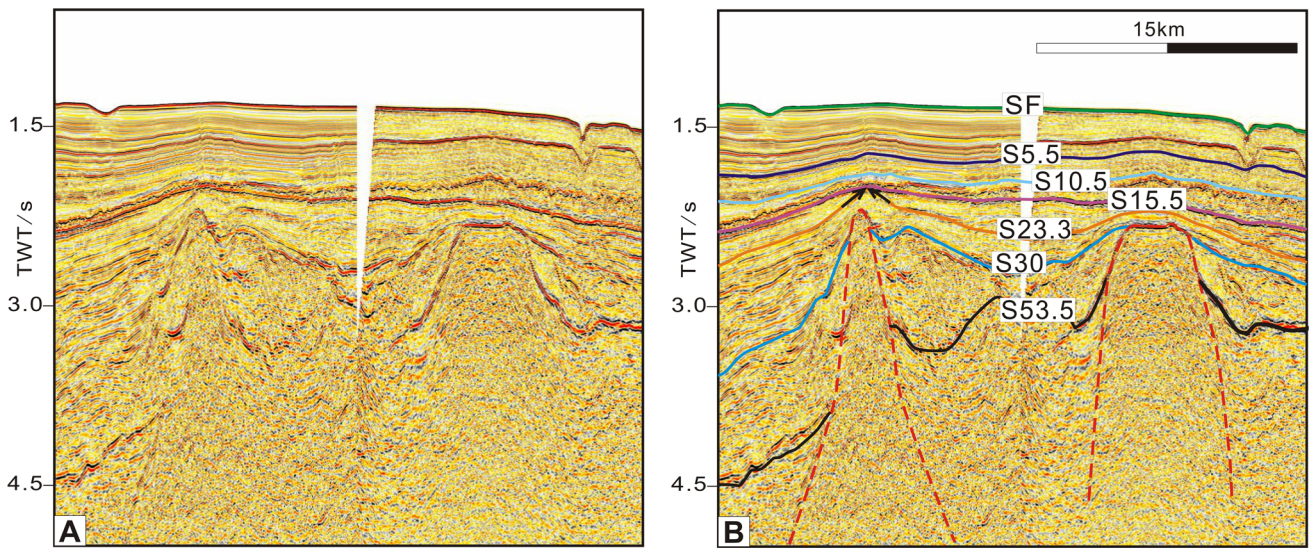

Fig. 14 Igneous rock formed during seafloor spreading (**A**) and its schematic illustration (**B**). Location of the seismic section displayed in (**A**) is shown in Fig. 2

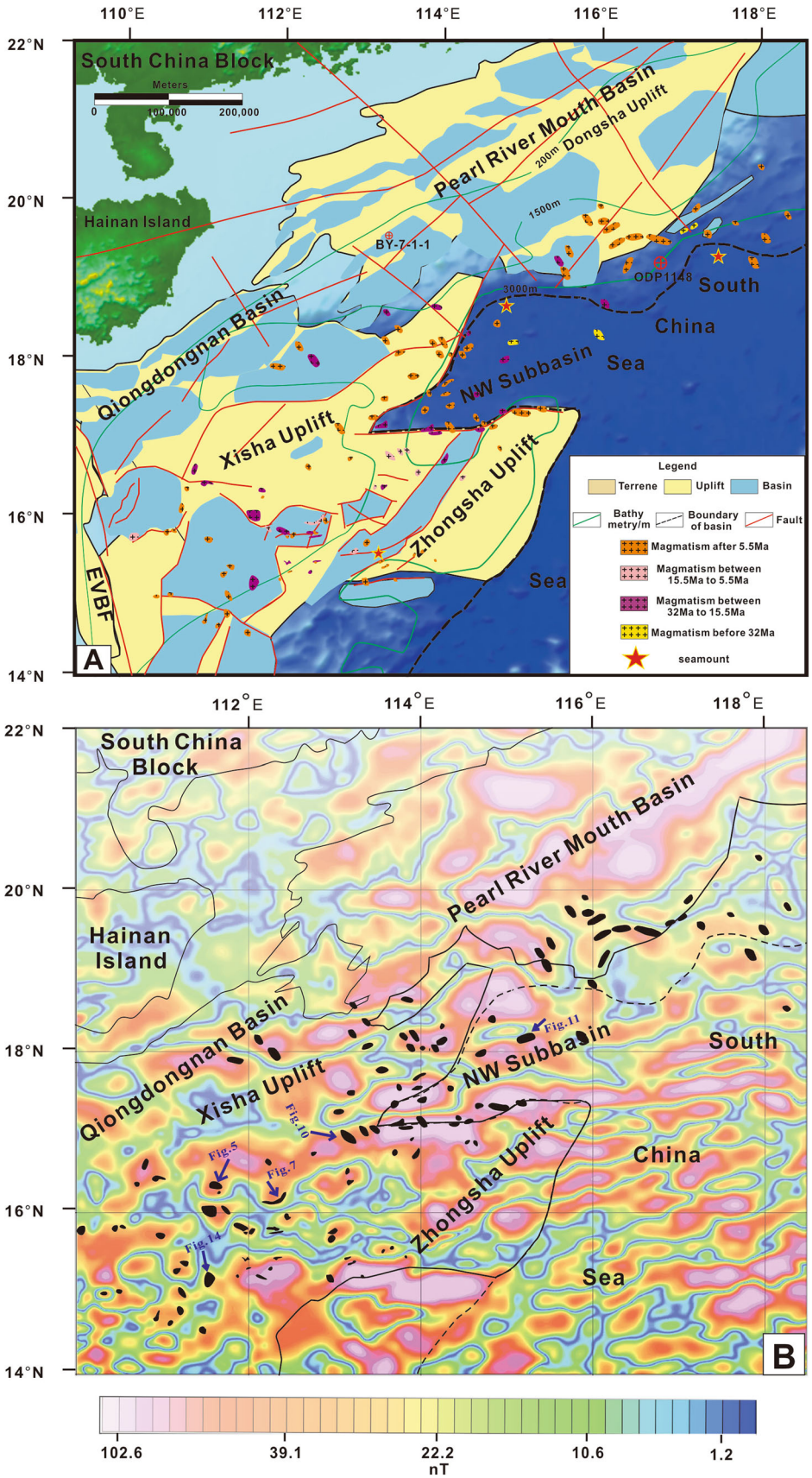
110°E
112°E
114°E
116°E
118°E
22°N
20°N
18°N
16°N
14°N
South China Block
Meters
0
100,000
200,000
Pearl River Mouth Basin
200m
Dongsha Uplift
1500m
Hainan Island
BY-7-1-1
ODP1148
3000m
South China Sea
Qiongdongnan Basin
NW Subbasin
Xisha Uplift
Zhongsha Uplift
EVBF
A
Legend
Terrene
Uplift
Basin
Bathy metry/m
Boundary of basin
Fault
Magmatism after 5.5Ma
Magmatism between 15.5Ma to 5.5Ma
Magmatism between 32Ma to 15.5Ma
Magmatism before 32Ma
seamount
112°E
114°E
116°E
118°E
22°N
20°N
18°N
16°N
14°N
South China Block
Pearl River Mouth Basin
Hainan Island
Qiongdongnan Basin
Xisha Uplift
NW Subbasin
South China Sea
Zhongsha Uplift
Fig.5
Fig.7
Fig.10
Fig.11
Fig.14
B
102.6
39.1
22.2
10.6
1.2
nT

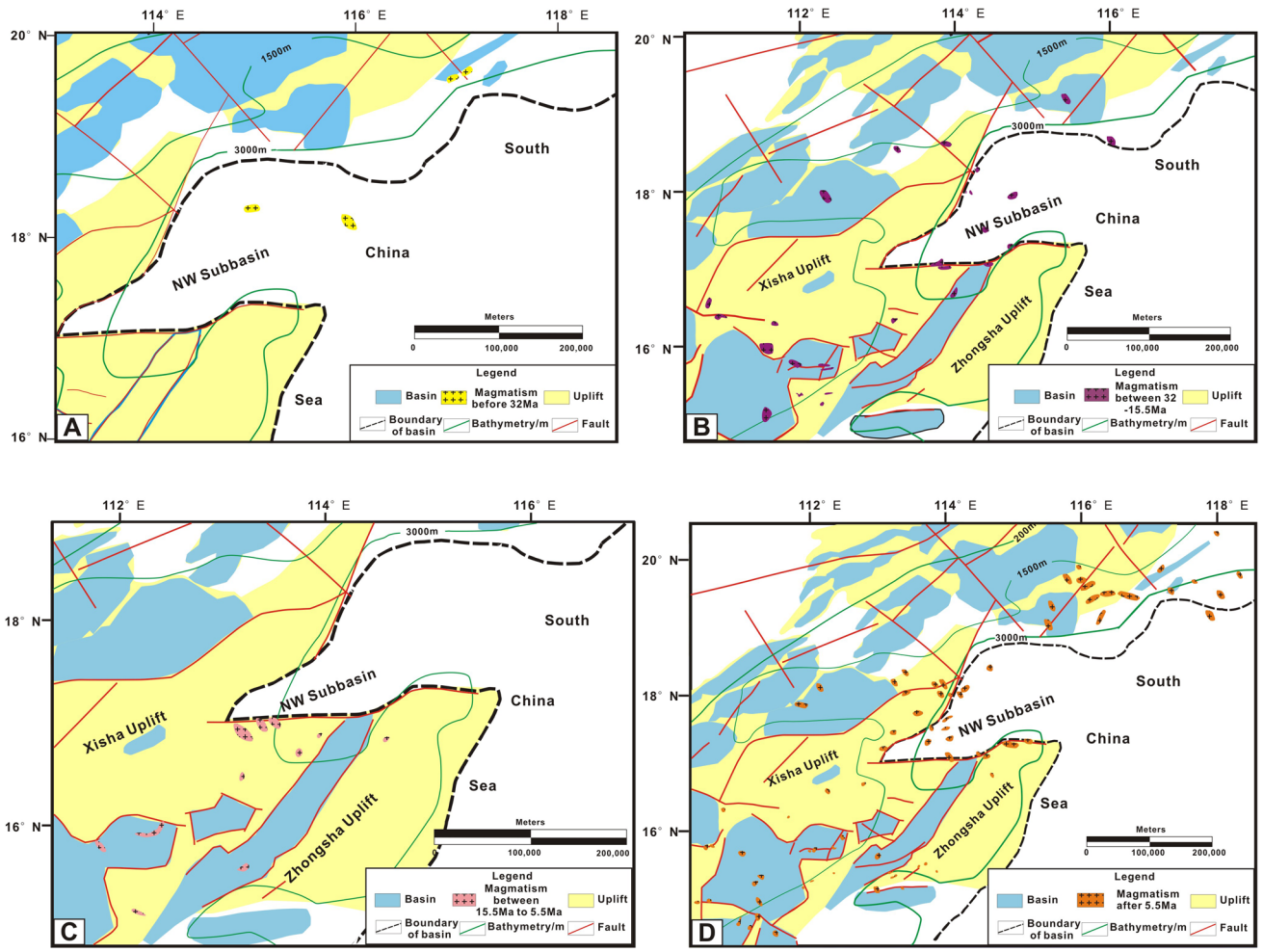

Fig. 16 Distribution of igneous rocks in the northern SCS margin at different periods. **A** >32 Ma: sporadic distribution in the southern Shenhu uplift and the NW subbasin. **B** 32–15.5 Ma: more intense magmatism than in the early Paleogene, distributed mainly on continental slopes, such as the Xisha areas. **C** 15.5–5.5 Ma: a few small igneous structures, scattered in the Xisha uplift and the NW subbasin. **D** 5.5 Ma—recent: magmatism occurs throughout the study area, smaller structures occur in the west

extensive magmatism. A great deal of magma intrusion occurred along nearly EW-trending tensile fractures and led to the formation of submarine seamounts in this period (Huang et al. 2001; Yan et al. 2001; Wu et al. 2014a, b). In addition to the study area, the main region of magmatism, the Leiqiong area generated igneous rocks that cover a surface up to 7000 km^2 (Flower et al. 1998; Ho et al. 2000), while the Indo-China Basalt Province covered an area of more than 8000 km^2 (Hoang et al. 1996; Hoang and Flower 1998). We collated the literature related to the chronological history of the SCS and found that most of the data relates to the time period between 5.5 Ma to recent (Table 1), possibly indicating a time delay in the plume-induced magmatism in the northern margin of the SCS.

It is worth noting that there was a strong post-rift tectonic event at ca. 5.5 Ma, with extensive crustal uplift and igneous activity. Although our results do not directly constrain the dynamic mechanism for tectonic movement, we speculate a relationship with lithospheric bending in this region. Such lithospheric bending is related to the initial collision of the North Luzon Arc with the East China continental margin, engulfing segments of the SCS along the northern Manila Trench (Lüdmann and Wong 1999; Lüdmann et al. 2001; McIntosh et al. 2013; Wu et al. 2014a, b). Following the major collision of Taiwan with the East China continental margin at the Miocene/Pliocene boundary, the NNW-WNW compression transforms to a WSW-SSW strike-slip motion along the northern margin of the SCS, giving rise to a transtensional neotectonic regime (Li 1993; Lüdmann and Wong 1999). Extension, induced by cooling of the oceanic crust and subduction at the Manila Trench, generated a transtensional tectonic regime which created or reactivated crustal zones of weakness and caused upwelling of mantle material (Lüdmann and Wong 1999; Lüdmann et al. 2001). At the same time, the Red River Shear Zone reversed from left- to right-lateral slip in

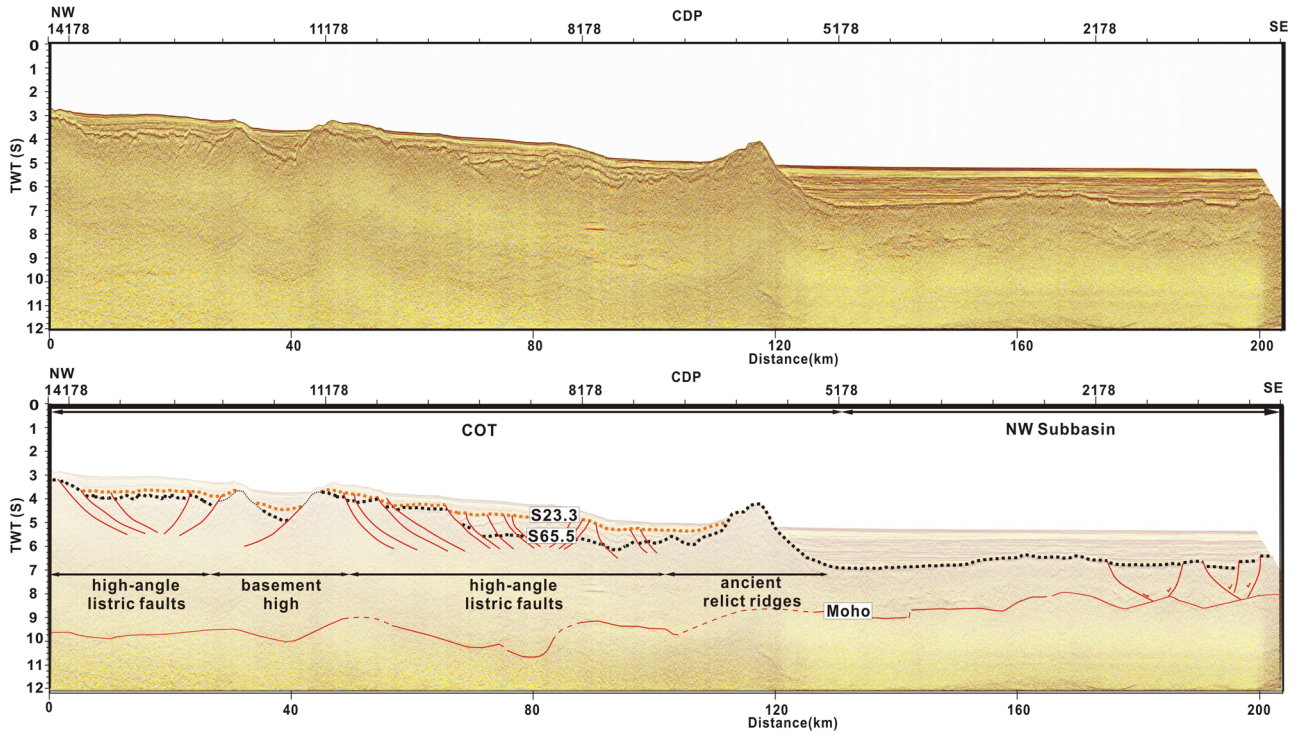

Fig. 17 Seismic profile showing thinning seaward. High-angle listric faults are widely present, the majority of which terminate in horizon S23.3, indicating the cessation of rifting in the basin. See Fig. 2 for location

response to the continuing India–Asia continental collision (Thi and Quan 1997; Zhu et al. 2009; Wang et al. 2013a, b). South-eastward extrusion of the South China Block eventually exceeded that of Indo-China in the late Neogene, causing strike-slip reversal of the Red River Shear Zone. Rapid subsidence, a rise of heat flow, a southeastward shift of the sedimentary depocenter and widespread volcanism took place in the areas which include (from south to north) central and southern Indo-China, Hainan Island, the Leizhou Peninsula, the Yinggehai Basin and the Qiongdongnan Basin along the seaward part of the Red River Shear Zone (Flower et al. 1998; Ho et al. 2000; Yan et al. 2006).The Hainan plume could have also been affected by this tectonic event along the northern margin of the SCS, becoming more active since 5.5 Ma. However, the specific cause of these sudden changes requires further discussion.

Classification of the northern rifted margin of the SCS

The most representative magma-poor margins are the Alpine Tethys and Iberia–Newfoundland rifted margins (which are characterized by thinned continental crust dissected by low-angle detachment faults and succeeded by exhumed sub-continental mantle (Dean et al. 2000; Reston and Phipps Morgan 2004; Péron-Pinvidic et al. 2007; Mohn et al. 2012). In this scenario, magmatism in the northern SCS was much more limited during continental breakup (White and McKenzie 1989), and gradually increased seaward. Another striking observation from several magma-poor margins is the delayed post-rift subsidence (Tucholke et al. 2007; Franke et al. 2014).

The northern SCS margin has been considered as a magma-poor rifted margin (Clift and Lin 2001; Yan et al. 2006; Franke et al. 2014; Gao et al. 2015). The following observations can be made from our research: (1) Igneous rocks associated with rifting are only found on the lower slope and apparently concentrate at the seaward edge of crustal blocks (Fig. 18). This result is consistent with the phenomenon observed in other areas, such as Dongsha, the Reed Bank and the Northwest Palawan Block (Clift and Lin 2001; Franke 2013). (2) High-angle listric faults developed in the northern margin of the SCS related to the fault-bounded rifted basin, most of which terminated at horizon S23.3 instead of S32 (Fig. 17), which is a seismic horizon marking the onset of seafloor spreading. This shows that rifting continued after seafloor spreading had begun, indicating a post-rift delay (Dong et al. 2008, 2014). (3) The thickness of the crust decreases sharply seaward, but no mantle exhumation is found (Figs. 17, 18). This can be explained by the observation of stretching factors (β) in the lower continental slope at ODP Site 1148 in between 2.5 and 3.5 (Clift and Lin 2001), implying the most highly stretched volcanic zone in the northern margin of the SCS. However, this continental thinning of the SCS was still not

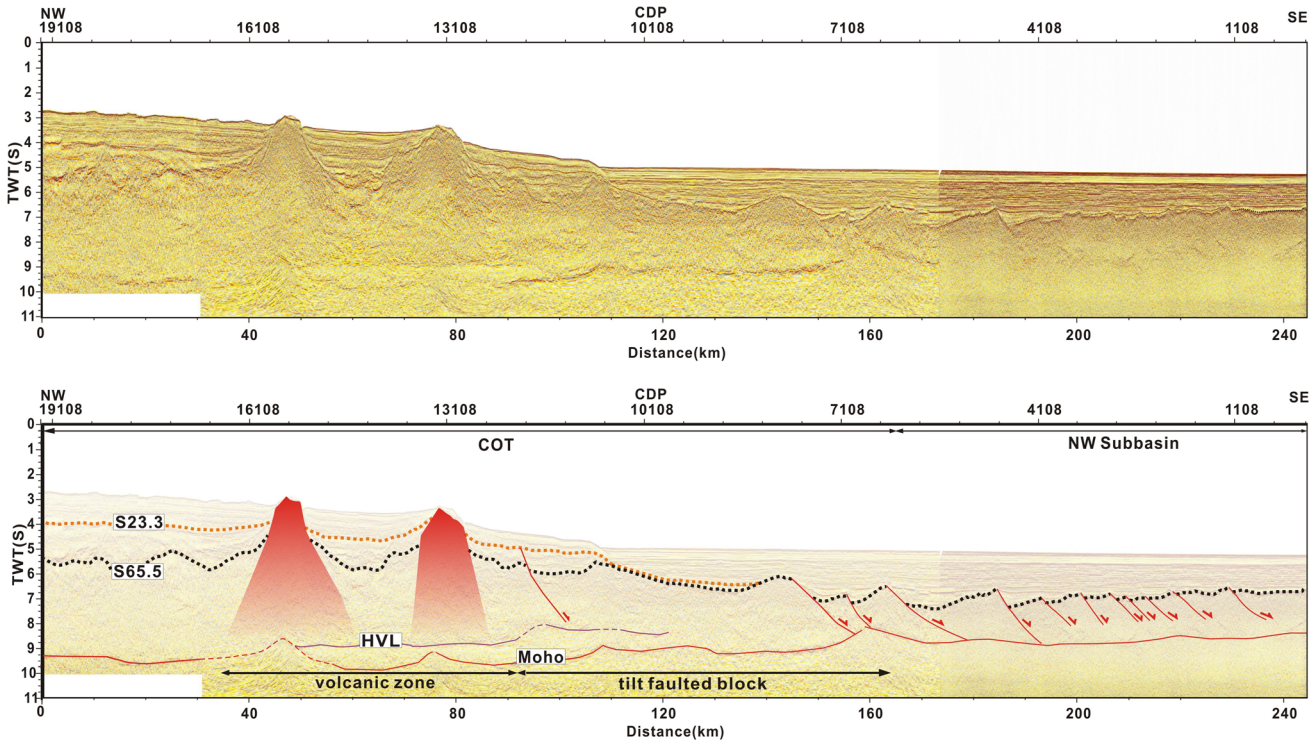

Fig. 18 Seismic profile showing low-angle top-basement faults which cut into mantle in the margin of the subbasin. Volcanoes are clearly concentrated at the seaward edge of the crustal blocks. See Fig. 2 for location

sufficient for mantle exhumation. (4) Similar to the other non-volcanic margins (Boillot et al. 1980; Perez-Gussinye et al. 2001; Whitmarsh et al. 2001), the northern margin of the SCS was not widely influenced by a mantle plume during rifting (Fig. 16A). Morley (2002) studied the rifted basins of SE Asia and found that the area affected by major magma intrusions may narrow during progressive extension of the continental crust, leading to a shift in deformation from the major boundary faults to minor fault swarms concentrated in narrow regions within the rifted depression. However, the characteristics of rifted depressions, such as the Baiyun sag in the northern margin of the SCS, is inconsistent with the evolutionary history described by Morley (2002) (Fig. 18). The northern margin of the SCS was rarely affected by extensive magmatism during the rifting phase.

The systematic assessment of the Cenozoic magmatism, from seismic profiles in the northern SCS supports the idea that the rifted margin of the northern SCS is a magma-poor margin, with absence of exhumed lithospheric mantle.

Conclusion

We set up the criteria for identifying the igneous rock structures in the northern margin of the SCS based on seismic profiles and drilling data. By analyzing the seismic features of these igneous rock structures and their relationship with adjacent strata we determine their mode and period of formation. The contact relationship with adjacent strata, sedimentary thickness on either side of the structure and seismic reflection characteristics are used as criteria to estimate the timing of igneous rock emplacement in seismic profiles. The main conclusions of this study are:

1. There are intrusive and extrusive rock structures in the northern margin of the SCS. Intrusive structures take different shapes depending on the magmatic energy. Extrusive structures are divided into flat-topped and conical-topped seamounts. Seismic characteristics are used to distinguish between buried volcanoes and intrusive rock structures: the overlying strata, the contact relationship and sills.
2. Cenozoic magmatism in the northern margin of the SCS is divided in three periods: before seafloor spreading (Paleocene and Eocene), during seafloor spreading (Early Oligocene–Mid Miocene) and after cessation of seafloor spreading (Mid Miocene–Recent). Magmatism occurred most extensively since 5.5 Ma, which can be regarded as a regionally remarkable event. The magmatism associated with the syn-rift stage in the northern SCS is extremely sporadic in seismic profiles, only found in the southern part of the PRMB and the NW subbasin.

3. The northern margin of the SCS can be defined as a magma-poor margin with absence of exhumed mantle as a special feature.

Acknowledgments We are grateful to CNOOC and PetroChina for their permission to release the seismic data. The constructive comments from both two anonymous reviewers and Guest Editor Hans Christian Larsen, Zhen Sun, Guoliang Zhang helped to revise this paper, they are also greatly appreciated. This research was supported by the Chinese National Scientific foundation (Nos. 91228208, 41476042, 40776036), the National Program on Key Basic Research Project of China (No. 2009CB219406), and the National High Technology Research and Development Program of China (No. 2009AA093401).

References

Anderson DL (1998) The edges of the mantle. In: Gurnis M et al (eds) The core-mantle boundary region. American Geophysical Union, Washington, pp 255–271

Barckhausen U, Roeser HA (2004) Seafloor spreading anomalies in the South China Sea revisited. In: Clift P, Wang P, Kuhnt W, Hayes D (eds) Continent–ocean interactions with East Asian Marginal Seas. American Geophysical Union 140:121–125

Barckhausen U, Engels M, Franke D, Ladage S, Pubellier M (2014) Evolution of the South China Sea: revised ages for breakup and seafloor spreading. Mar Pet Geol 58:599–611

Bellon H, Rangin C (1991) Geochemistry and isotopic dating of Cenozoic volcanic arc sequences around the Celebes and Sulu seas. ODP Scientific Results, Leg, 124

Boillot G, Grimaud S, Mauffret A, Mougenot D (1980) Ocean–continent boundary off the Iberian Margin: a serpentinite diapir west of the Galicia Bank. Earth Planet Sci Lett 48(1):27–34

Briais A, Patriat P, Tapponnier P (1993) Updated interpretation of magnetic anomalies and seafloor spreading stages in the South China Sea: implications for the Tertiary tectonics of Southeast Asia. J Geophys Res 98(B4):6299–6328

Campbell IH, O'Neill SCH (2012) Evidence against a chondritic earth. Nature 483:553–558

Charvet J, Lapierre H, Yu YW (1994) Geodynamic significance of the Mesozoic volcanism of southeastern China. J SE Asian Earth Sci 9:387–396

Chung SL, Cheng HC, Jahn BM, O'Reilly SY, Zhu BQ (1997) Major and trace element, and Sr–Nd isotope constraints on the origin of Paleogene volcanism in South China prior to the South China Sea opening. Lithos 40:203–220

Clift P, Lin J (2001) Preferential mantle lithospheric extension under the South China margin. Mar Pet Geol 18:929–945

Clift P, Lin J, Barckhausen U (2002) Evidence of low flexural rigidity and low viscosity lower continental crust during continental break-up in the South China Sea. Mar Pet Geol 19:951–970

Clift P, Lee HG, Duc NA, Barckhausen U, Long HV, Sun Z (2008) Seismic reflection evidence for a Dangerous Grounds miniplate: no extrusion origin for the South China Sea. Tectonics 27(TC3008):1–16

Davies RJ, Bell BR, Cartwright JA, Shoulders S (2002) Three-dimensional seismic imaging of Palaeocene dike-fed submarine volcanoes from the northeast Atlantic margin. Geology 30:223–226

Dean SM, Minshull TA, Whitmarsh RB, Louden K (2000) Deep structure of the ocean–continent transition in the southern Iberia Abyssal Plain from seismic refraction profiles: II The IAM-9 transect at 408 209 N. J Geophys Res 105:5859–5886

Deniz C, Senay H, Dae CK, Gwang HL, Hyun CH, Moo HK (2010) The distribution and characteristics of the igneous complexes in the northern East China Sea Shelf Basin and their implications for hydrocarbon potential. Mar Geophys Res 31:299–313

Dong DD, Wu SG, Zhang GC, Yuan SQ (2008) Rifting process and formation mechanisms of syn-rift stage prolongation in the deepwater basin, northern South China Sea. Chin Sci Bull 53(23):3715–3725

Dong DD, Wu SG, Li JB, Lüdmann T (2014) Tectonic contrast between the conjugate margins of the South China Sea and the implication for the differential extensional model. Sci China (Earth Sci) 57(6):1415–1426

Expedition 349 Scientists (2014) South China Sea tectonics: opening of the South China Sea and its implications for southeast Asian tectonics, climates, and deep mantle processes since the late Mesozoic. IODP Preliminary Report, 349, pp 1–109. doi:10.14379/iodp.pr.349.2014

Flower MFL, Tamaki K, Hoang N (1998) Mantle extrusion: a model ford is persed volcanism and DUPAL-like asthenosphere in East Asia and the western Pacific, in Mantle Dynamics and Plate Interactions in East Asia. Geodyn Ser 27:67–88

Franke D (2013) Rifting, lithosphere breakup and volcanism: comparison of magma-poor and volcanic rifted margins. Mar Pet Geol 43:63–87

Franke D, Savva D, Pubellier M, Steuer S, Mouly B, Auxiêtre J-L, Meresse F, Chamot-Rooke N (2014) The final rifting evolution in the South China Sea. Mar Pet Geol 58:704–720

Gao JW, Wu SG, McIntosh K, Mi LJ, Yao BC, Chen ZM, Jia LK (2015) The continent–ocean transition at the mid-northern margin of the South China Sea. Tectonophysics. doi:10.1016/j.tecto.03.003

Hansen DM (2006) The morphology of intrusion-related vent structures and the their implications for constraining the timing of intrusive events along the NE Atlantic margin. J Geol Soc 163:789–800

Hansen DM, Redfern J, Federici F, di Biase D, Bertozzi G (2008) Miocene igneous activity in the Northern Subbasin, offshore Senegal, NW Africa. Mar Pet Geol 25:15

Hart SR, Hauri EH, Oschmann LA, Whitehead JA (1992) Mantle plumes and entrainment: isotopic evidence. Science 256:517–520

Hauri EH, Whitehead JA, Hart SR (1994) Fluid dynamic and geochemical aspects of entrainment in mantle plumes. J Geophys Res 99:24275–24300

Hinz K, Schlüter HU (1985) Geology of the dangerous grounds, South China Sea, and the continental margin off southwest Palawan: results of Sonne cruises SO-23 and SO-27. Energy 10:282–288

Ho KS, Chen JC, Juang WS (2000) Geochronology and geochemistry of late Cenozoic basalts from the Leiqiong area, southern China. J Asian Earth Sci 18:307–324

Hoang N, Flower MFL (1998) Petrogenesis of Cenozoic Basalts from Vietnam: implication for origins of a diffuse Igneous Province. J Petrol 39(3):369–395

Hoang N, Flower MFJ, Carlson RW (1996) Major, trace element, and isotopic compositions of Vietnamese basalts: interaction of hydrous EM1-rich asthenosphere with thinned Eurasisn lithosphere. Geochim Cosmochim Acta 60(22):4329–4351

Holloway NH (1982) North Palawan Block, Philippines—its relation to Asian mainland and role in evolution of South China Sea. AAPG Bulletin 66:1355–1383

Huang CY, Xia KY, Yuan PB (2001) Structural evolution from Paleogene extension to Latest Miocene—recent arc-continent

collision offshore Taiwan: comparison with on land geology. J Asian Earth Sci 19(5):619–639
Huang ZC, Wang LS, Zhao DP, Xu MJ, Mi N, Yu DY, Li H, Li C (2010) Upper mantle structure and dynamics beneath Southeast China. Phys Earth Planet Inter 182:161–169
Jackson CAL (2012) Seismic reflection imaging and controls on the preservation of ancient sill-fed magmatic vents. J Geol Soc 169:503–506
Jahn BM, Zhou XH, Li JL (1990) Formation and tectonic evolution of southeastern China and Taiwan: isotopic and geochemical constraints. Tectonophysics 183:145–160
Jia DC, Qiu XL, Hu RZ, Lu Y (2003) Geochemical nature of mantle reservoirs and tectonic setting of basalts in Beibu Gulf and its adjacent region. J Trop Oceanogr 22(2):30–39
Jin XL (1989) The geosciences research report in South China Sea. Donghai Mar Sci 7(4):30–42 **(in Chinese abstract)**
Keen CE, Dehler SA (1993) Stretching and subsidence: rifting of conjugate margins in the North Atlantic region. Tectonics 12:1209–1229
Kudrass HR, Wiedicke M, Cepek P (1986) Mesozoic and Cenozoic rocks dredged from the South China Sea (Reed Bank area) and Sulu Sea and their significance for plate-tectonic reconstructions. Mar Pet Geol 3:9–30
Lebedev S, Nolet G (2003) Upper mantle beneath Southeast Asia from S velocity tomography. J Geophys Res: Sol Earth 108(B1)
Lebedev S, Chevrot S, Nolet G, van Hilst RD (2000) New seismic evidence for a deep mantle origin of the S. China basalts (the Hainan Plume?) and other observations in SE Asia. Eos Trans AGU 81:48
Lee GH, Watkins JS (1998) Seismic sequence stratigraphy and hydrocarbon potential of the Phu Khanh Basin offshore central Vietnam, South China Sea. AAPG Bulletin 82:1711–1735
Lee GH, Kwon YI, Yoon CS, Kim HJ, Yoo HS (2006) Igneous complexes in the eastern Northern South Yellow Sea Basin and their implications for hydrocarbon systems. Mar Pet Geol 23(6):631–645
Lei JS, Zhao DP, Steinberger B, Wu B, Shen FL, Li ZL (2009) New seismic constraints on the upper mantle structure of the Hainan plume. Phys Earth Planet Inter 173:33–50
Lei C, Ren JY, Clift PD (2011) The structure and formation of diapirs in the Yinggehai-Song Hong Basin, South China Sea. Mar Pet Geol 28:980–991
Li PL (1993) Cenozoic tectonic movement in the Pearl River Mouth Basin. China Offshore Oil Gas (Geol) 7:11–17 **(in Chinese with English abstract)**
Li PL, Rao CT (1994) Tectonic characteristics and evolution history of the Pearl River Mouth basin. Tectonophysics 235(1–2):13–25
Li ZL, Qiu ZL, Qin SX, Pang X, Liang D, Teng Y, Li Y (1991) A study on the forming conditions of basalts in seamounts of the South China Sea. Acta Mineral Sin 11(4):325–334 **(in Chinese with English abstract)**
Li CN, Wang FZ, Zhong CS (2005) Geochemistry of Quaternary basaltic volcanic rocks of Weizhou island in Beihai City of Guangxi and a discussion on characteristics of their source. Act Petrol Mineral 24(1):1–11 **(in Chinese with English abstract)**
Li S, Meng X, Guo L, Yao C, Chen Z, Li H (2010) Gravity and magnetic anomalies field characteristics in the South China Sea and its application for interpretation of igneous rocks. Appl Geophys 7(4):295–305
Li CF, Xu X, Lin J, Sun Z, Zhu J, Yao YJ, Zhao XX, Liu QS, Kulhanek DK, Wang J, Song T, Zhao JF, Qiu N, Guan YX, Zhou ZY, Williams T, Bao R, Briais A, Brown EA, Chen YF, Clift PD (2014) Age and magnetic structures of the South China Sea constrained by deep tow magnetic surveys and IODP Expedition 349. Geochem Geophys Geosyst 15(12):4958–4983
Lin CS, Gao JY, Yu XJ, Ye F, Tan YJ (2006) Characteristics of tectonic movement in the northern part of South China Sea during the Cenozoic. Acta Oceanol Sin 28(4):81–86
Lüdmann T, Wong HK (1999) Neotectonic regime on the passive continental margin of the northern South China Sea. Tectonophysics 311:113–138
Lüdmann T, Wong HK, Wang P (2001) Plio-Quaternary sedimentation processes and neotectonics of the northern continental margin of the South China Sea. Mar Geol 172:331–358
Maruyama S (1994) Plume tectonics. J Geol Soc 100:24–49
McDermott F, Defant MJ, Hawkesworth CJ, Maury RC, Joron JL (1993) Isotope and trace element evidence of three component mixing in the genesis of the North Luzon arc lavas (Philippines). Contrib Mineral Petrol 113:9–23
McIntosh K, van Avendonk H, Lavier L, Lester WR, Eakin D, Wu F, Liu CS, Lee CS (2013) Inversion of a hyper-extended rifted margin in the southern Central Range of Taiwan. Geology 41(8):871–874
Meng X, Guo L, Chen Z, Li S, Shi L (2009) A method for gravity anomaly separation based on preferential continuation and its application. Appl Geophys 6(3):217–225
Mohn G, Manatschal G, Beltrando M, Masini E, Kusznir N (2012) Necking of continental crust in magma-poor rifted margins: evidence from the fossil Alpine Tethys margins. Tectonics 31(1):TC1012
Montelli R, Nolet G, Dahlen FA (2006) A catalogue of deep mantle plumes: new results from finite frequency tomography. Geochem Geophys Geosyst 7(11):1–69
Morley CK (2002) A tectonic model for the Tertiary evolution of strike—slip faults and rift basins in SE Asia. Tectonophysics 347:189–215
Nolet G, Karato SI, Montelli R (2006) Plume fluxes from seismic tomography. Earth Planet Sci Lett 248:685–699
Pang X, Yang SK, Zhu M (2004) Deep-water fan systems and petroleum resources on the Northern Slope of the South China Sea. Acta Geol Sin-Engl Edit 78(3):626–631
Pautot G, Rangin C, Briais A (1990) The axial ridge of the South China Sea: a seabeam and geophysical survey. Oceanol Acta 13(2):129–143
Perez-Gussinye M, Reston TJ, Phipps Morgan J (2001) Rheological and magmatic evolution during extension at passive nonvolcanic margins: the effect of initial lithospheric structure. In: Wilson RCL et al (eds) Nonvolcanic rifting of continental margins: a comparison of evidence from land and sea. Geol Soc [Lond] Spec Publ 187:551–576
Péron-Pinvidic G, Manatschal G, Minshull T, Sawyer D (2007) The tectono sedimentary and morpho-tectonic evolution recorded in the deep Iberia–Newfoundland margins: evidence for a complex break-up history. Tectonics 10:TC001970
Pigott JD, Ru K (1994) Basin superposition on the northern margin of the South China Sea. Tectonophysics 235:27–50
Planke S, Symonds PA, Alvestad E, Skogseid J (2000) Seismic volcanostratigraphy of large-volume basaltic extrusive complexes on rifted margins. J Geophys Res 105(8):335–351
Qin GQ (2007) A discussion on age of the Zhuhai formation and Neogene-Paleogene boundary in the Pearl River Mouth Basin. China Offshore Oil Gas 19(1):1–9 **(in Chinese with English abstract)**
Rangin C, Klein M, Roques D, Pichon XL, Trong LV (1995) The Red River fault system in the Tonkin Gulf, Vietnam. Tectonophysics 243:209–222
Rao CT, Li PL (1991) On the heat flow in PRMB. China Offshore Oil and Gas (Geol) 5(6):7–18 **(in Chinese with English abstract)**
Reston TJ, Phipps Morgan J (2004) Continental geotherm and the evolution of rifted margins. Geology 32(2):133–136

Ru K, Pigott JD (1986) Episodic rifting and subsidence in the South China Sea. AAPG Bull 70(9):1136–1155

Shi HS, Li CF (2012) Mesozoic and early Cenozoic tectonic convergence to rifting transition prior to opening of the South China Sea. Int Geol Rev 54(15):1801–1828

Shi XF, Yan QS (2011) Geochemistry of Cenozoic magmatism in the South China Sea and its tectonic implications. Mar Geol Quat Geol 31(2):59–72 **(in Chinese with English abstract)**

Sohn YK (1996) Hydro volcanic processes forming basaltic tuff ring sand cones on Cheju Island, Korea. Geol Soc Am Bull 108:1199–1211

Sun Z, Zhou D, Wu SM, Zhong ZH, Jiang JQ (2009) Patterns and dynamics of rifting on passive continental margin from shelf to slope of the Northern South China Sea: evidence from 3D analogue modeling. J Earth Sci 20(1):136–146

Sun QL, Wu SG, Lüdmann T, Wang B, Yang TT (2011) Geophysical evidence for cyclic sediment deposition on the southern slope of Qiongdongnan Basin, South China Sea. Mar Geophys Res 32:415–428

Sun QL, Wu SG, Cartwright J, Lüdmann T, Yao GS (2013) Focused fluid flow systems of the Zhongjiannan Basin and Guangle Uplift, South China Sea. Basin Res 25:97–111

Svensen H, Planke S, Malthe-Sørenssen A, Jamtveit B, Myklebust R, Eidem TR, Rey SS (2004) Release of methane from a volcanic basin as a mechanism forinitial Eocene global warming. Nature 429:542–545

Tapponnier P, Peltzer G, Le Dain Y, Armijo R, Cobbold P (1982) Propagating extrusion tectonic in Asia: new insights from simple experiments with plasticine. Geology 10:611–616

Tapponnier P, Peltzer G, Armijo R (1986) On the mechanics of the collision between India and Asia. Geol Soc Lond Spec Publ 19:115–157

Taylor B, Hayes DE (1983) Origin and history of the South China Sea basin. In: Hayes DE (eds) The tectonic and geologic evolution of Southeast Asian Seas Islands, Part 2[A]. AGU, Washington. Geophys Monogr 27: 23–56

Thi P, Quan T (1997) Dynamic role of the Red River Fault; orogenic uplift and basin subsidence. J Geol Ser B 9–10:33–46

Trude KJ, Cartwright JA, Davies RJ, Smallwood JR (2003) New technique fordating igneous sills. Geology 31:813–816

Tucholke BE, Sawyer DS, Sibuet JC (2007) Breakup of the Newfoundland-Iberia rift. In Karner G, Manatschal G, Pinheiro LD (eds) Imaging, mapping and modelling continental lithosphere extension and breakup. Geol Soc Lond Spec Publ 9–46

Uyeda S, Miyashiro A (1974) Plate tectonics and the Japanese Islands: a synthesis. Bull Geol Soc Am 85:1159–1170

Wan L, Yao BC, Zeng WJ (2006) Lithospheric structure and petroleum distribution in the South China Sea. Geol China 33(4):814–884 **(in Chinese with English abstract)**

Wang SS, Chen SZ (1999) Geological features of Cenozoic basins offshore China. In: Qiu Zhongjian, Gong Zaisheng (eds) Petroleum Exploration in China. Oil Industry Press, Beijing, p 922

Wang XJ, Wu MQ, Liang DH, Yin AW (1984) Some geochemical characteristics of basalts from the South China Sea. Geochemica 4:332–340 **(in Chinese with English abstract)**

Wang P, Prell WL, Blum P, Arnold EM, Buehring CJ, Chen MP, Clemens SC, Clift PD, Colin CJG, Farrell JW, Higginson MJ, Jian Z, Kuhunt W, Laj CE, Lauer-Leredde C, Leventhal JS, Li A, Li Q, Lin J, McIntyre K, Miranda CR, Nathan SA, Shyu J-P, Solheid PA, Su X, Tamburini F, Trentesaux A, Wang L (2000) In: Proceedings of the Ocean Drilling Program, initial reports, 184. Ocean Drilling Program, College Station, TX 2000

Wang TK, Chen MK, Lee CS, Xia KY (2006) Seismic imaging of the transitional crust across the Northeastern Margin of the South China Sea. Tectonophysics 412:237–254

Wang DW, Wu SG, Qin ZL (2013a) Seismic characteristics of the Huaguang mass transport deposits in the Qiongdongnan Basin, South China Sea: implications for regional tectonic activity. Mar Geol 346:165–182

Wang XC, Li ZX, Li XH, Li J, Xu YG, Li XH (2013b) Identification of an ancient mantle reservoir and young recycled materials in the source region of a young mantle plume: implications for potential linkages between plume and plate tectonics. Earth Planet Sci Lett 377–378:248–259

Wei KS, Cui HY, Ye SF (2001) High-precision sequence stratigraphy in Qiongdongnan basin. Earth Sci-J China Univ Geosci 20(1):59–66 **(in Chinese with English abstract)**

White R, McKenzie D (1989) Magmatism at rift zone: the generation of volcanic continental margins and flood basalts. J Geophys Res 94:7685–7729

Whitmarsh RB, Manatschal G, Minshull TA (2001) Evolution of magma-poor continental margins from rifting to seafloor spreading. Nature 413:150–154

Wu SG, Yang Z, Wang DW, Lv FL, Lüdmann T, Craig F, Wang B (2014a) Architecture, development and geological control of the Xisha carbonate platform, northwestern South China Sea. Mar Geol 350:71–83

Wu SG, Gao JW, Zhao SJ, Lüdmann T, Chen DX, Spence G (2014b) Post-rift uplift and focused fluid flow in thepassive margin of northern South China Sea. Tectonophysics 615–616:27–39

Yan P, Liu HL (2004) Tectonic–stratigraphic division and blind fold structures in Nansha waters, South China Sea. J Asian Earth Sci 24:337–348

Yan QS, Shi XF (2007) Hainan mantle plume and the formation and evolution of the South China Sea. Geol J Chin Univ 13(2):311–322 **(in Chinese with English Abstract)**

Yan QS, Shi XF (2009) Characteristics of volcaniclastic rocks from seamounts in the South China Sea and its geological implications. Acta Petrol Sin 25(12):59–73 **(in Chinese with English abstract)**

Yan P, Zhou D, Liu ZS (2001) A crustal structure profile across the northern continental margin of the South China Sea. Tectonophysics 338:1–21

Yan P, Deng H, Liu HL, Zhang ZR, Jiang YK (2006) The temporal and spatial distribution of volcanism in the South China Sea region. J Asian Earth Sci 27:647–659

Yan QS, Shi XF, Wang QS, Pu WR, Xiao L (2008) Major element, trace element, Sr–Nd–Pb isotopic studies of Cenozoic alkali basalts from the South China Sea. Sci China (Ser D) 51(4):550–566 **(in Chinese with English abstract)**

Yan QS, Shi XF, Castillo PR (2014) The late Mesozoic-Cenozoic tectonic evolution of the South China Sea: apetrologic perspective. J Asian Earth Sci 85:178–201

Yao BC, Zeng WJ, Chen YZ, Zhang XL (1994) Xisha trough of South China Sea-an ancient suture. Mar Geol Quat Geol 14(1):1–10 **(in Chinese with English abstract)**

Yeh YC, Sibuet JC, Hsu SK, Liu CS (2010) Tectonic evolution of the North-eastern South China Sea from seismic interpretation. J Geophys Res 115(B06103):1–21

Zhang WY, Zhang FY, Yang KH, Hu GD, Yang SX, Cheng YS, Zhao GJ (2007) Fractal characteristics of resource quantity of cobalt crusts and seamount topography, the West Pacific. Front Earth Sci China 1(2):233–240

Zhang GL, Smith-Duque C, Tang SH, Li H, Zatikian C, D'Hondt S, Inagaki F (2012) Geochemistry of basalts from IODP site U1365: implications for magmatism and mantle source signatures of the mid-Cretaceous Osbourn Trough. Lithos 144–145:73–87

Zhao DP (2004) Global tomographic images of mantle plumes and subducting slabs: insight into deep Earth dynamics. Phys Earth Planet Inter 146(1–2):3–34

Zhao DP (2007) Multiscale seismic tomography of mantle plumes and subducting slabs. In: Yuen D, Maruyama S (eds) Superplumes: beyond Plate Tectonics. Springer, Berlin, pp 7–30

Zhao MH, Qiu XL, Xia SH, Xu HL, Wang P, Wang TK, Lee CS, Xia KY (2010) Seismic structure in the northeastern South China Sea: S-wave velocity and Vp/Vsratios derived from three-component OBS data. Tectonophysics 480:183–197

Zhao DP, Yu S, Ohtani E (2011) East Asia: seismotectonics, magmatism and mantle dynamics. J Asian Earth Sci 40:689–709

Zhou XM, Li WX (2000) Origin of late Mesozoic igneous rocks in southeastern China: implications for lithosphere subduction and underplating of mafic magmas. Tectonophysics 326:269–287

Zhou D, Liu HL, Chen HZ (2005) Mesozoic-Cenozoic magmatism in southern South China Sea and its surrounding areas and its implications to tectonics. Geotecton Metallog 29(3):354–363

Zhou XM, Sun T, Shen WZ, Shu LS, Niu YL (2006) Petrogenesis of Mesozoic granitoids and volcanic rocks in South China: a response to tectonic evolution. Episodes 29:26–33

Zhu MZ, Graham S, McHargue T (2009) The Red River Fault zone in the Yinggehai Basin, South China Sea. Tectonophysics 476(3–4):397–417

Zou HP (1993) Episodes and distribution of Cenozoic volcanism in northern part of South China Sea and Taiwan strait as well as their neighboring areas. J East China Geol Inst 16(1):24–31

Zou H, Fan Q (2010) U-Th isotopes in Hainan basalts: implications for subasthenospheric origin of EM2 mantle end member and the dynamics of melting beneath Hainan Island. Lithos 116:145–152

Zou HP, Li PL, Rao CT (1995) Geochemistry of Cenozoic volcanic rocks in Pearl River Mouth Basin and its geodynamic significance. Geochemica 24(Suppl):33–45 **(in Chinese with English abstract)**